AFGL-TR-88-0170

INFLUENCE OF SCATTERING ON SEISMIC WAVES.

M. Nafi Toksöz
Anton M. Dainty

Earth Resources Laboratory
Department of Earth, Atmospheric, and
Planetary Sciences
Massachusetts Institute of Technology
Cambridge, Massachusetts 02139

8 August 1988

Final Report
30 January 1986—30 January 1988

Air Force Geophysics Laboratory
Air Force Systems Command
United States Air Force
Hanscom Air Force Base, Massachusetts 01731

Sponsored by:
DARPA Order No.
Monitored by:
Contract No.

Defense Advanced Research Projects Agency
Nuclear Monitoring Research Office
5299
Air Force Geophysics Laboratory
F19628-86-K-0004

The views and conclusions contained in this document are those of the authors and should not be interpreted as representing the official policies, either expressed or implied, of the Defense Advanced Research Projects Agency or the US Government.

"This technical report has been reviewed and is approved for publication"

JAMES F. LEWKOWICZ
Contract Manager
Solid Earth Geophysics Branch
Earth Sciences Division

HENRY A. OSSING
Chief
Solid Earth Geophysics Branch
Earth Sciences Division

FOR THE COMMANDER

DONALD H. ECKHARDT, Director
Earth Sciences Division

This document has been reviewed by the ESD Public Affairs Office (PA) and is releasable to the National Technical Information Service (NTIS).

Qualified requestors may obtain additional copies from the Defense Technical Information Center. All others should apply to the National Technical Information Service.

If your address has changed, or if you wish to be removed from the mailing list, or if the addressee is no longer employed by your organization, please notify AFGL/DAA, Hanscom AFB, MA 01731-5000. This will assist us in maintaining a current mailing list.

Do not return copies of this report unless contractual obligations or notices on a specific document requires that it be returned.

unclassified
SECURITY CLASSIFICATION OF THIS PAGE

AD-A201 120

REPORT DOCUMENTATION PAGE

1a. REPORT SECURITY CLASSIFICATION unclassified	1b. RESTRICTIVE MARKINGS
2a. SECURITY CLASSIFICATION AUTHORITY	3. DISTRIBUTION / AVAILABILITY OF REPORT Approved for public release; distribution unlimited
2b. DECLASSIFICATION / DOWNGRADING SCHEDULE	
4. PERFORMING ORGANIZATION REPORT NUMBER(S)	5. MONITORING ORGANIZATION REPORT NUMBER(S) AFGL-TR-88-0170
6a. NAME OF PERFORMING ORGANIZATION Earth Resources Laboratory Dept. of Earth, Atmospheric, and Planetary Sciences 6b. OFFICE SYMBOL (If applicable)	7a. NAME OF MONITORING ORGANIZATION Air Force Geophysics Laboratory
6c. ADDRESS (City, State, and ZIP Code) Massachusetts Institute of Technology Cambridge, MA 02139	7b. ADDRESS (City, State, and ZIP Code) Hanscom AFB, MA 01731
8a. NAME OF FUNDING / SPONSORING ORGANIZATION 8b. OFFICE SYMBOL (If applicable)	9. PROCUREMENT INSTRUMENT IDENTIFICATION NUMBER F19628-86-K-0004
8c. ADDRESS (City, State, and ZIP Code)	10. SOURCE OF FUNDING NUMBERS

PROGRAM ELEMENT NO	PROJECT NO.	TASK NO.	WORK UNIT ACCESSION NO
61101E	6A10	DA	BF

11. TITLE (Include Security Classification)
Influence of Scattering on Seismic Waves (unclassified)

12. PERSONAL AUTHOR(S)
M. Nafi Toksöz, Anton M. Dainty

13a. TYPE OF REPORT	13b. TIME COVERED	14. DATE OF REPORT (Year, Month, Day)	15. PAGE COUNT
Final	FROM 1/30/86 TO 1/30/88	1988 August 8	100

16. SUPPLEMENTARY NOTATION

17. COSATI CODES		
FIELD	GROUP	SUB-GROUP

18. SUBJECT TERMS (Continue on reverse if necessary and identify by block number)
coda, scattering, array analysis, phase velocity, attenuation, Rg

19. ABSTRACT (Continue on reverse if necessary and identify by block number)

Work on this contract has examined two subjects, the analysis of seismic data using the NORESS array in southern Norway and the attenuation properties of the crust. As our final report we present two preprints of papers submitted or in press. The first, "Phase velocity estimation of diffusely scattered waves", by A.M. Dainty and D.B. Harris, has been submitted to the Bulletin of the Seismological Society of America. It deals with the work at NORESS which was partly carried out under a previous contract, partly in conjunction with the Lawrence Livermore National Laboratory and partly under this contract. The second paper, "A model for attenuation and scattering in the earth's crust", by M.N. Toksöz, A.M. Dainty, E. Reiter and R.-S. Wu, is in press in PAGEOPH. It describes the work on attenuation and was supported by the US Geological Survey and this contract.

20. DISTRIBUTION / AVAILABILITY OF ABSTRACT	21. ABSTRACT SECURITY CLASSIFICATION
☒ UNCLASSIFIED/UNLIMITED ☐ SAME AS RPT ☐ DTIC USERS	unclassified

22a. NAME OF RESPONSIBLE INDIVIDUAL	22b. TELEPHONE (Include Area Code)	22c. OFFICE SYMBOL
James F. Lewkowicz	617/377-3028	LWH

DD FORM 1473, 84 MAR 83 APR edition may be used until exhausted
All other editions are obsolete

SECURITY CLASSIFICATION OF THIS PAGE
unclassified

TABLE OF CONTENTS

PREFACE

Work on this contract has examined two subjects, the analysis of data using the NORESS array in southern Norway and the attenuation properties of the crust. As our final report we present two preprints of papers submitted or in press. The first, "Phase velocity estimation of diffusely scattered waves", by A. M. Dainty and D. B. Harris, has been submitted to the Bulletin of the Seismological Society of America. It deals with the work at NORESS, which was partly carried out under a previous contract, partly in conjunction with the Lawrence Livermore National Laboratory and partly under this contract. The second paper, "A model for attenuation and scattering in the earth's crust", by M. N. Toksöz, A. M. Dainty, E. Reiter and R.-S. Wu, is in press in PAGEOPH. It describes the work on attenuation and was supported by the U. S. Geological Survey and this contract.

PHASE VELOCITY ESTIMATION OF DIFFUSELY SCATTERED WAVES

by

Anton M. Dainty*

Earth Sciences Division/LWH
Air Force Geophysics Laboratory
Hanscom AFB MA 01731-5000

David B. Harris

L-205
Lawrence Livermore National Laboratory
P. O. Box 808
Livermore CA 94550

Submitted to
Bulletin of the Seismological Society of America

March 1988

*Also at:

Earth Resources Laboratory
Dept. Earth, Atmospheric, and Planetary Sciences
Massachusetts Institute of Technology
Cambridge MA 02139

ABSTRACT

Two methods are investigated for estimating the phase velocity of diffusely scattered seismic waves simultaneously arriving from different azimuths and recorded by a two-dimensional array of seismometers. The Hankel spectrum is the average of the frequency-wavenumber (FK) spectrum over all azimuths, while the wavenumber spectrum is derived by integrating the FK spectrum around a contour of constant phase velocity, i.e., a circle centered on the origin in the wavenumber plane. If the conventional estimate of the FK spectrum using the covariance matrix of the seismometer signals is integrated, a closed form for both the Hankel spectrum and the wavenumber spectrum may be found; the two spectra are very similar, the wavenumber spectrum being equal to the Hankel spectrum times the wavenumber. In spite of this similarity, however, we find that the two formulations have significantly different behaviour for small wavenumbers, i.e., high phase velocities. In both cases there is a highest (true) velocity that can be estimated from the spectral maximum for a given array aperture ("velocity cutoff"). The Hankel spectrum estimates too high a velocity; for true wavenumbers below a certain limit infinite velocity is estimated. The wavenumber spectrum, on the other hand, estimates too low a velocity, and there is an upper limit on the estimated velocity. An example illustrating these difficulties for the two methods is given for teleseismic P coda of an event recorded at the NORESS array in southern Norway: in spite of the problems, the analysis is able to demonstrate that the

coda consists of two components, a coherent P wave component with a high phase velocity and a diffuse S wave component of low phase velocity. The cutoff and bias problem are investigated by numerical simulation for the NORESS array using azimuthal averaging and synthetic signals. The results confirm and quantify the cutoff problem at low wavenumbers and indicate that wavenumbers estimated from the Hankel and wavenumber spectra maxima bracket the true wavenumber, with the Hankel spectrum estimate being low (phase velocity too high) and the wavenumber spectrum estimate high. The bias of both methods decreases with increasing wavenumber (decreasing phase velocity) and they are both asymptotically unbiased. The wavenumber spectrum has a superior performance at low wavenumbers (high phase velocity), but the Hankel spectrum gives superior results at high wavenumbers (low phase velocity). The product of the linear wavenumber (= 1/wavelength) and the array aperture define "high" and "low" wavenumbers; for low wavenumbers the product is 1 or less. In an Appendix we find absolute lower bounds on the cutoffs analytically. The problems could be mitigated by using high resolution methods.

INTRODUCTION

With a two-dimensional array of seismometers it is possible to determine the phase velocity (i.e., the velocity at which wavefronts sweep across the array) and azimuth of seismic waves recorded by the array; Lacoss *et al.* (1969) describe some of the commonly used techniques for accomplishing this. Generally, most methods have concentrated on making as complete a determination as possible. One of the most useful concepts has been estimation of the frequency-wavenumber (FK) spectrum, which is the power spectrum in frequency and two wavenumber components of the seismic wavefield considered as a function of time t and two space coordinates x and y. This is equivalent to decomposing the observed wavefield into plane waves with a range of azimuth from 0 to 360° and a range of phase velocities from 0 to ∞ for the case of a continuous array. Specifically, at a specified angular frequency ω a point k_x, k_y in the plane defined by two wavenumbers corresponds to an azimuth θ measured from the y (North) axis given by

$$\tan\theta = k_x \; k_y \tag{1}$$

and a phase velocity C,

$$C = \omega \; k \tag{2}$$

where the scalar wavenumber k is given by

$$k^2 = k_x^2 + k_y^2 \tag{3}$$

Henceforth k will be referred to as simply the wavenumber. If the plane wave is interpreted as a wave of velocity V incident at an angle i to the vertical (z) axis,

$$C = V / \sin i \tag{4}$$

Note that (4) implies

$$C \geq V \tag{5}$$

The decomposition into plane waves represented by the FK spectrum has great usefulness if the wavefield can be considered as being due to a source or sources sufficiently far from the array for wavefront curvature to be ignored. Then significant energy from azimuth θ can be interpreted as coming from a source situated along azimuth θ. The phase velocity can often be used to identify the wave type (from (5)) and calculate its angle of incidence for a body wave. However, some difficulties have emerged. One of these is the case of more than one source or wave type, especially when one of the sources or wave types is dominant and the others weak. While some successes have been reported (Lacoss *et al.*, 1969; Capon *et al.*, 1969) using analysis methods that retain a complete separation of all of the variables of the FK spectrum, another possibility is averaging over some of the variables to increase the reliability and signal to noise ratio of relevant aspects of the data. Nawab *et al.* (1985) introduced the zero-delay wavenumber spectrum, which is theoretically equivalent to summing the FK spectrum over all frequencies. In addition, Nawab *et al.* integrated the zero-delay spectrum along lines of constant azimuth; by (1) these are straight lines passing

radially outwards from the wavenumber origin. In this manner these authors were able to estimate the azimuth of sources using information from all frequencies and phase velocities present in the data.

In this paper we are interested in determining the phase velocity of waves recorded at an array averaged over all azimuths. This problem has been examined by Haubrich and McCamy (1969) and Iyer and Healy (1972) in analyses of seismic noise. Haubrich and McCamy introduce the Hankel spectrum, which is the average of the FK spectrum over all θ at fixed k and ω. We have conducted a theoretical evaluation of the resolution of this method and a very similar formulation we have developed to estimate the power in a window at time t as a function of wavenumber k; such an estimate will be referred to as a wavenumber spectrum. The evaluation indicates that while both methods have difficulties at high phase velocities if the conventional FK spectrum is used as the basis of the estimation, the wavenumber spectrum is superior. The problem at high phase velocity is due to the lack of resolution of the conventional FK spectrum. The Hankel spectrum, however, gives superior results for low phase velocities. We confirm these results numerically for the NORESS array geometry (Bungum *et al.*, 1985; Figure 1). Iyer and Healy (1972) derive an approximate method to find the dominant wavenumber k using signals from an array which consists of seismometers at the vertices of a hexagon surrounding a central seismometer. We have not examined this method because we are interested in a more general analysis.

To illustrate the application of the two formalisms we show an example using the seismic problem of teleseismic P coda. This example shows the problems at high phase velocities and is presented before the theoretical discussion of these problems to provide a practical demonstration of them. Figure 2 shows the signal received at the center seismometer of the NORESS array in southern Norway from a suspected underground nuclear test in East Kazahkstan at 38° distance. The large pulse delineated by the earliest 5 s window is the direct P wave from the source to the receiver. A model for the energy ("coda") following this first arrival has been proposed (Dainty, 1988). The model hypothesizes that the coda consists of two components due to scattering in the crust near the source and receiver respectively. The portion of the coda due to source scattering will have approximately the same phase velocity and azimuth as the direct wave and will be coherent across the array. Scattering near the receiver, on the other hand, will produce waves having the full range of azimuths 0 to 360° and phase velocities typical of crustal phases. Since this component at any instant of time consists of a number of waves of different azimuth and phase velocity, it will not be coherent across the array; it is in this sense that it may be described as "diffusely scattered". The Hankel and wavenumber spectra are applied to this problem using the data shown in Figure 2.

THEORY

In order to detect the presence of scattered P and S waves in the coda, we propose to investigate how coda energy is distributed in slowness (wavenumber). Since scattered waves may be approaching from a wide range of azimuths, it is appropriate to integrate the energy contributions at a particular slowness over all azimuths. By scanning over slowness, one may attempt to detect peaks in energy at the slowness values which correspond to P and S wave propagation.

Let us denote the signal received at a single sensor by $s(t)$. Since an array is a collection of sensors, the received signal is a vector waveform, which we call $\underline{s}(t)$. We assume further that the data are available in digitized form:

$$s[n] = s(t_0 + n\Delta t) \tag{6}$$

where we use the square brackets to denote a discrete index, and Δt to denote the sampling interval.

Following Capon (1969), the conventional FK spectrum is a discrete Fourier transform in the wavenumber domain, operating on the monochromatic spatial covariance matrix $\underline{R}(\omega)$, with elements $R_{mn}(\omega)$:

$$P(k,\theta) = \sum_{m=1}^{M} \sum_{n=1}^{M} e^{jk\hat{d}^T(\theta)x_m} R_{mn}(\omega) e^{-jk\hat{d}^T(\theta)x_n} \tag{7}$$

$P(k, \theta)$ is defined in terms of the azimuth θ, the direction cosine vector

$$\underline{d}(\theta) = \begin{bmatrix} \cos\theta \\ \\ \sin\theta \end{bmatrix} \tag{8}$$

and the wavenumber k. The locations of the M sensors in the array are denoted by the vectors $\underline{x}_i$.

In practice, the monochromatic covariance matrix is estimated through a direct Fourier transform of the vector signal:

$$\underline{R}(\omega) = \sum_{i=1}^{L} \underline{v}_i(\omega)\, \underline{v}_i^H(\omega) \tag{9}$$

where

$$v_i(\omega) = A_i \sum_{n=0}^{N-1} s[n + (i-1)N]\, e^{-j\omega n \Delta t} \tag{10}$$

It is common practice (Capon (1969)) to average the covariance matrix estimate over multiple windows in order to make it full-rank and to reduce the variance of the estimate. The L windows may be weighted differently with the weighting function A_i. Since our interest is in the structure of the coda, and since the amplitude of the coda decays exponentially with time (Dainty, 1988), we have made the weighting inversely proportional to a decaying exponential fit to the envelope of the coda:

$$A_i = A \left[e^{-\alpha(i-1)N\Delta t} \right]^{-1} \tag{11}$$

We have chosen α to fit the exponential to the coda envelope, and A so that:

$$\sum_i A_i = 1. \tag{12}$$

Circular Contour Integrals

To examine the contribution of diffusely scattered waves to the coda we want to integrate the FK spectrum (7) around contours of constant phase velocity. Since we are estimating a monochromatic FK spectrum, contours of constant phase velocity are circles in the wavenumber plane. Haubrich and McCamy (1969) proposed the Hankel spectrum, which is the average of the FK spectrum over all θ at a given k:

$$\overline{H}(k) = \frac{1}{2\pi} \int_{-\pi}^{\pi} P(k,\theta)\ d\theta \tag{13}$$

We shall examine this statistic and a very similar one we shall call the wavenumber spectrum, which is proportional to the energy in the FK spectrum at wavenumber k over all θ:

$$\overline{P}(k) = \frac{1}{2\pi} \int_{-\pi}^{\pi} P(k,\theta)\ k\, d\theta \tag{14}$$

The expression $kd\theta$ in (14) is the line element on the circle of integration in the wavenumber plane, since we wish to find the total energy. Note that, since k does not depend on θ,

$$\overline{P}(k) = k\overline{H}(k) \tag{15}$$

These integrals can be evaluated in closed form for $P(k,\theta)$ given by (7) (Haubrich and McCamy, 1969) by transforming the difference in sensor locations into polar coordinates:

$$x_m - x_n = \rho_{mn} \begin{bmatrix} \cos(\psi_{mn}) \\ \sin(\psi_{mn}) \end{bmatrix} \tag{16}$$

where

$$\rho_{mn} = \sqrt{(\underline{x}_m - \underline{x}_n)^T(\underline{x}_m - \underline{x}_n)} \tag{17}$$

is the magnitude of the difference vector, and ψ_{mn} is the angle between $\underline{x}_m$ and $\underline{x}_n$. Then using:

$$d^T(\theta)(x_m - x_n) = \rho_{mn}\cos(\theta - \psi_{mn}) \tag{18}$$

and the integral representation for the zeroth order Bessel function J_0:

$$\frac{1}{2\pi}\int_{-\pi}^{\pi} e^{jk\underline{d}^T(\theta)(\underline{x}_m - \underline{x}_n)}\, d\theta = J_0(k\rho_{mn}) \tag{19}$$

Haubrich and McCamy obtain the Hankel spectrum as:

$$H(k) = \sum_{m=1}^{M}\sum_{n=1}^{M} R_{mn}(\omega)J_0(k\rho_{mn}) \tag{20}$$

We observe that (20) can be computed directly from the covariance matrix, without an intermediate computation of the FK spectrum itself. Using (15) we see immediately that the wavenumber spectrum is given by:

$$P(k) = k\sum_{m=1}^{M}\sum_{n=1}^{M} R_{mn}(\omega)J_0(k\rho_{mn}) \tag{21}$$

Due to the fact that the Bessel function evaluations may be computationally expensive, one may wish to exploit symmetries in the matrix to reduce the number of evaluations. Making use of

$$R_{mn}(\omega) = R^*_{nm}(\omega) \tag{22}$$

and

$$\rho_{nn} = 0 \tag{23}$$

the number of evaluations may be reduced by more than a factor of two:

$$\overline{P}(k) = k \sum_{m=1}^{M} R_{mm}(\omega) + 2k \sum_{m=1}^{M} \sum_{n=m+1}^{M} Re\{R_{mn}(\omega)\} J_0(k\rho_{mn}) \tag{24}$$

with a similar expression for $\overline{H}(k)$.

EXAMPLE

In this section we present an application of the Hankel and wavenumber spectra to the event shown in Figure 2 and compare the results with FK analysis. As a result of this comparison we note that the phase velocity determined by a finite array is biased towards high values (i.e., low wavenumbers) for the Hankel spectrum and towards low values (i.e., high wavenumbers) for the wavenumber spectrum. These biases effectively constitute a "velocity estimation cutoff" in the sense that they effectively prevent the estimation of true velocities higher than a certain value, which differs for the two spectra. We investigate the effect further in the following section both theoretically and using synthetic data and numerical techniques.

Two sets of windows, 5 s long, are shown in Figure 2. The first set consists of a single window around first P. The second set covers the coda from 20 to 100 s after first P. This time interval contains the arrival PP (surface reflected P), but the power in this phase is not large. To improve the reliability of the frequency-wavenumber and wavenumber spectra for the coda, estimates have been made for each 5 s window and then averaged over all windows after multiplication of each estimate by the weight given by (11) above. This procedure assumes that the coda is statistically stationary (Dainty, 1988).

Figure 3 shows FK spectra for first P and the coda. In this Figure and succeeding Figures and discussion, linear wavenumber $K = k/(2\pi)$ will often be used. The spectra are

taken at the peak frequency of the first P, which is also the peak frequency of the coda. The first P shows a prominent peak at $C = 15.5$ km/s, $\theta = 85°$, close to the expected values of 13.2 km/s and 78°. No other significant energy is evident in the first P window. The coda FK spectrum also shows a peak at $C = 11.7$ km/s and $\theta = 70°$. This peak indicates there is a coherent part of the coda due to scattering near the source. The difference between the phase velocity and azimuth of the first P and the coda is probably due to the combined effects of local scattering distorting the wavefronts, the small size of the array, the use of only one window for first P, and contamination of the coda peak by energy with slower phase velocities and off-source azimuths. There is some evidence of a diffuse component of the coda consisting of slower waves coming from different azimuths, but it is not possible to determine the phase velocity or the relative importance of this component from Figure 3.

In Figures 4 and 5 we present the Hankel and wavenumber spectra, respectively, corresponding to the FK spectra of Figure 3. Both the spectra for first P and for coda are dominated by a peak at $K = 0$, or infinite phase velocity. From synthetic examples, this peak is interpreted as being due to the high velocity component seen in Figure 3, but the position of the peak is biased towards low wavenumbers (high phase velocities) by the weighting effect of the Bessel function in (20) towards the origin of wavenumber, where it has a maximum. Careful comparison of the first P and coda Hankel spectra shows that there is an excess of higher wavenumbers in the coda relative to first P, indicating that there is some low phase velocity energy present in the coda as well as the high phase velocity

component.

The wavenumber spectra in Figure 5 show a prominent peak for the first P window at linear wavenumber 0.2 km^{-1} (C = 9 km/s); this peak is interpreted as corresponding to the peak at C = 15.5 km/s seen in Figure 3, but with a bias towards lower phase velocities (higher wavenumbers). Note that due to the multiplier k in (15) there cannot be a peak at the origin of wavenumber for the wavenumber spectrum. There is a secondary peak at a linear wavenumber of 0.7 km^{-1} (C = 2.6 km/s); this is apparently a sidelobe of the main peak due to the finite aperture and spatial sampling of the array. This identification is confirmed by synthetic examples discussed later. The coda wavenumber spectrum shows a peak at wavenumber 0.25 km^{-1} (C = 7.2 km/s), similar to the values for the first P window. Comparing this result with Figure 3, the coda peak at 0.25 km^{-1} corresponds to the peak in the frequency-wavenumber spectrum at C = 11.7 km/s and $\theta = 70°$, and represents the coherent part of the coda due to scattering near the source. Differences from the peak in the first P window are attributed to the same factors as for the frequency-wavenumber spectra of Figure 3.

However, in Figure 5 it is clearly seen that the coda contains a component with higher wavenumbers (lower phase velocities) than the first P, with a broad peak at a wavenumber of 0.55 km^{-1} (C = 3.3 km/s). This peak is not present in the first P window or for the synthetic examples and is at a different wavenumber than the sidelobe seen in the first P window and the synthetic examples. There is no single prominent peak in Figure 3 with this

phase velocity. A phase velocity of 3.3 km/s is characteristic of horizontally propagating S waves or surface waves. To arrive so soon after first P, such waves must have been generated near the array. This peak is thus identified with a diffusely scattered component of the coda consisting of shear or surface waves arriving from many different azimuths due to scattering with phase velocities between 3 and 4 km/s. Since the wavenumber spectrum gives an estimate of the energy present at a given wavenumber, comparing first P and coda spectra in Figure 5 indicates that the diffusely scattered component appears to be about as strong as the coherent component for this event.

In summary, the analysis using the wavenumber spectrum has successfully separated the coda into near source and near receiver scattered components. However, a bias towards high wavenumbers (low phase velocity) was noted. The FK spectrum analysis did not separate the components clearly because of the diffuse nature of the near receiver component. The Hankel spectrum analysis encountered difficulty due to a bias towards low wavenumbers (high phase velocity) which led to domination of the spectra by the high phase velocity near source component. In the next section we examine the issue of bias, which first became evident in analyses such as those presented above.

VELOCITY ESTIMATOR BIAS

Both the Hankel and wavenumber spectra can be used as estimators of phase velocity. Since they are estimators of average or total energy respectively as a function of wavenumber, by finding a maximum of energy, we obtain an estimate of wavenumber (and for monochromatic signals, phase velocity). The performance of estimators is usually characterized by two quantities: bias and variance. In this section we address the question of bias, leaving the variance to a future publication.

The Hankel and wavenumber integrals have nearly identical form, but exhibit different bias. We use both because the estimates they provide bracket the true wavenumbers (and phase velocities) of incident waves. In addition, we demonstrate that bias is controlled by array aperture. For arrays of limited aperture, the bias problem becomes acute at small wavenumbers, culminating in an estimation cutoff. The existence of a cutoff means that wavenumbers below a calculable threshold cannot be estimated. In an Appendix, an absolute lower bound on this threshold which depends only on aperture is obtained analytically for arrays exhibiting near-circular symmetry. In this section we numerically evaluate the expected bias and the exact cutoff for the NORESS array geometry, and confirm the calculations using synthetic signals.

The cutoff phenomenon is examined by considering the spectra generated by plane waves incident on the array. Suppose a plane wave is incident from direction θ_o with angular

frequency ω and phase velocity C. The theoretical covariance matrix for the wavefield is:

$$R_{mn}(\omega) \quad = \quad E\, e^{j \frac{\omega}{C} \underline{d}^T(\theta_o)\,(\underline{x}_m \,-\, \underline{x}_n)} \tag{25}$$

where E is the energy density of the wave. The Hankel and wavenumber spectra are:

$$\overline{P}(k) \quad = \quad k\,E \sum_{m=1}^{M} \sum_{n=1}^{M} e^{j \frac{\omega}{C} \underline{d}^T(\theta_o)\,(\underline{x}_m \,-\, \underline{x}_n)}\, J_0(k\rho_{mn}) \quad = \quad k\,\overline{H}(k) \tag{26}$$

These spectra should be approximately independent of the direction of approach, θ_o, for arrays with nearly circularly symmetric geometry such as NORESS (Figure 1). Indeed, NORESS was designed to have uniform performance over all azimuths. Instead of picking a particular direction for our analysis, we examine the average spectra:

$$\langle \overline{P}(k) \rangle \quad = \quad \frac{1}{2\pi} \int_{-\pi}^{\pi} \overline{P}(k)\, d\theta_o \tag{27}$$

$$= \quad k \cdot H(k) \tag{28}$$

Because of the rotational symmetry of the problem, the average spectra should be approximately equal to the spectra obtained for a particular direction of approach: consequently, the estimated wavenumbers and biases should be approximately the same. The average spectra are:

$$\langle \overline{P}(k) \rangle \quad = \quad k\,E \sum_{m=1}^{M} \sum_{n=1}^{M} J_0(k \cdot \rho_{mn})\, J_0(k\rho_{mn}) \tag{29}$$

$$= \quad k \cdot H(k) \tag{30}$$

where

$$k \cdot \quad = \quad \frac{\omega}{C} \tag{31}$$

From these analytic expressions for the spectra, the wavenumbers that would be estimated from the spectral maxima for incident plane waves having true wavenumber k^*, or true linear wavenumber K^*, can be calculated numerically for the NORESS geometry. In Figure 6, these maxima wavenumbers for the azimuthally averaged Hankel and wavenumber spectra are plotted as a function of K^* over the range 0 to 1 cycle/km. The cutoff effect discussed earlier is clearly seen near $K^* = 0$: for the Hankel spectrum a value of 0 is estimated for any value of K^* less than ~ 0.22, while for the wavenumber spectrum the estimated value at $K^* = 0$ is ~ 0.17. Indeed, generally the wavenumber spectrum estimate is biased high and the Hankel spectrum estimate is biased low. As previously noted, they jointly bracket the true wavenumber.

To assure that the azimuthally averaged spectra provide wavenumber estimates close to those obtained for individual plane waves, we computed estimates for synthetic signals representing single plane waves with a dominant frequency of 1 or 2 Hz incident from due North with a specified phase velocity. Figure 7 shows the Hankel and wavenumber spectra for a 2 Hz signal with a phase velocity of 23 km/s. Note the similarity of the results for this high phase velocity signal to the first P spectra in Figures 4 and 5. Maxima estimates for a suite of phase velocities from such synthetic cases are plotted on Figure 6 and agree well with the averaged spectra results, certifying the averaging approach. In fact, the approach of using the azimuthally averaged spectra may be more correct for coda scattering investigations, since waves may be expected to arrive over a band of directions.

The implications of this analysis for velocity estimation are more readily appreciated in Figure 8. In this Figure, the wavenumber estimates are reinterpreted as velocity estimates for the two cases $f = 1.0$ Hz and $f = 2.0$ Hz. The true velocity is bounded from above by the Hankel spectrum estimate and from below by the wavenumber spectrum estimate. Low velocities are estimated well, but the spectra provide no constraints in the high velocity range. With increasing frequency the constraints improve, i.e., velocity resolution increases with frequency, because at a given phase velocity the wavenumber is higher at higher frequencies by (2).

As mentioned previously, the cutoff problem is examined analytically in an Appendix. By setting $\rho_{mn} = \Delta$, where Δ is the diameter (aperture) of the array, it may be shown that the Hankel spectrum will have a peak at $k = 0$ for all

$$k < \alpha \Delta \tag{32}$$

where $\alpha \approx 2.4$. Since actually $\rho_{mn} \leq \Delta$, this is a lower bound on the cutoff for the Hankel spectrum. Similarly, the wavenumber spectrum cannot have a peak at wavenumbers below

$$k_{min} = \beta \Delta \tag{33}$$

where $\beta \approx 1.2$. Again, this is a lower bound. Remembering that $k = \omega / C$, the maximum phase velocity that can be estimated by the wavenumber spectrum is determined from:

$$\frac{\omega}{C} \Delta = \beta \tag{34}$$

i.e.

$$C_{max} \approx \frac{\omega\Delta}{1.2} \tag{35}$$

For the Hankel spectrum, the cutoff is defined by:

$$C_{max} \approx \frac{\omega\Delta}{2.4} \tag{36}$$

The two theoretical wavenumber cutoffs implied by (32) and (33) are indicated on Figure 6. It is clear that the actual NORESS cutoffs occur at higher wavenumbers. This confirms that the minimum theoretical wavenumbers are lower bounds which will not be attained by any realizable array. The disparity occurs because in a realizable array all of the ρ_{mn} cannot be equal to the array aperture as was assumed in the analysis. However, although the bounds are optimistic, they do establish the existence of the cutoff phenomenon.

The cutoffs can be understood intuitively with the help of Figure 9. This Figure shows the FK spectrum for a pure plane wave coming from the North with a true linear wavenumber $K^* = 0.1$ cycles/km, within both cutoffs. The spectrum is estimated by computing the beampattern and shifting it by 0.1 cycles/km Northward to emphasise the influence of the width of the main lobe of the beampattern on the cutoff. The dashed circles represent contours of integration in (13) and (14). The inner circle passes through the peak of the FK spectrum; if there were no cutoffs and no bias, both the Hankel spectrum (13) and the wavenumber spectrum (14) would have their maxima for this circle of integration. The outer dashed circle is at the cutoff radius for the wavenumber spectrum, $K = 0.17$. Considering

first the Hankel spectrum, the value obtained for the inner, true, circle will be the average around the circle by (13). But we see that this is probably less than the value at the origin, $K = 0$, because the value at the origin is ~ 500, and most of the circle passes through regions of the FK spectrum that have lower values (the peak of the spectrum is normalized to the square of the number of array elements, $25^2 = 625$). Our analysis using (30) and synthetic signals presented in Figure 6 shows that in fact the peak of the Hankel spectrum lies at the origin. For the wavenumber spectrum, the integration around the dashed circular contours is weighted by the factor k, the radius of the circle of integration. Because of this, it is quite possible that the largest value of the wavenumber spectrum will lie at a greater value of K than the true value shown by the inner dashed circle in Figure 9. The results summarized in Figure 6 show that the largest value actually occurs for the outer dashed circle.

The crucial factor in the argument presented in the preceding paragraph is the role played by the finite width of the main lobe of the beampattern caused by the finite aperture of the array. If the array had infinite aperture, the broad peak seen in Figure 9 would become a very narrow peak concentrated near the true value indicated by the cross. Then both the Hankel and the wavenumber spectra would have their peaks at the true wavenumber because there would only be significant power near this wavenumber. Instead, the lack of resolution of the actual array causes energy in the FK spectrum to be spread to lower and higher wavenumbers, with the results noted above for sufficiently small wavenumbers. We

shall return to this question of resolution later.

One final method of viewing the bias problem is instructive. In Figure 10 we have plotted the normalized velocity bias, defined as:

$$\frac{C_{est} - C_{true}}{C_{true}} = \frac{1/K_{est} - 1/K}{1/K} \tag{37}$$

as a function of the aperture expressed as a fraction of horizontal wavelength λ, $\Delta/\lambda = \Delta K$. The Hankel spectrum bias exhibits the cutoff very clearly with a vertical asymptote at small aperture. The biases of both methods become acceptably small as the aperture exceeds one wavelength, which is a restatement of the classical Rayleigh resolution limit. Below one wavelength, the wavenumber spectrum has smaller bias, and may be usable down to about half a wavelength. The relative performance of the Hankel and wavenumber spectra at low wavenumbers agrees with the results (35) and (36) as well as our practical experience as shown in the Example section. Above one wavelength, the Hankel spectrum generally has less bias, though both methods are asymptotically unbiased.

A final important point that must be made is that the analysis of this velocity cutoff has been explicitly carried out for the formulations (24) and (20) which were based on the conventional FK estimate (7), and would not apply to the contour integrals (13) and (14) based on some other FK estimate. Indeed, both methods are constrained by the classical Rayleigh resolution limit. The existence of higher resolution methods, such as the Maximum Likelihood Method (Capon, 1969), suggests that the constraint may be eased, reducing the

bias, and extending the analysis to higher velocities. We will report on this possibility in a future publication.

DISCUSSION AND CONCLUSIONS

Two methods have been evaluated to find the phase velocity of waves from two-dimensional array data when the wavefield consists of waves arriving simultaneously from different azimuths. The first method, the Hankel spectrum of Haubrich and McCamy (1969), is the average of the FK spectrum over all azimuths at a constant wavenumber. The second formulation, called the wavenumber spectrum, is derived by integrating the FK spectrum around circles centered on the origin in wavenumber space, i.e., contours of constant phase velocity. If the conventional estimate of the FK spectrum using the covariance matrix of the seismometer signals is used, the resulting integrals may be evaluated in closed form. The two expressions that result are very similar: if k is the wavenumber, the wavenumber spectrum is k times the Hankel spectrum.

The spectra have been used to examine teleseismic P coda using the NORESS array. The wavenumber spectrum demonstrates that the coda consists of a high phase velocity P wave component scattered near the source and a low phase velocity S wave component scattered near the receiver. However, a bias effect at high phase velocities was noted; for the Hankel spectrum there was also a bias of such severity that useful results could not be obtained. The sense of the bias was different for the two formulations, leading to high phase velocities for the Hankel spectrum and low phase velocities for the wavenumber spectrum. For both formulations the problem appeared to culminate in a velocity cutoff, i.e., there

was a highest (true) phase velocity that could be estimated.

To investigate the problem further and explain the different results obtained by the two methods we undertook theoretical and numerical studies. The apparently slight difference in the formulations has a pronounced effect near $k = 0$, i.e., high phase velocities. The wavenumber spectrum is zero at $k = 0$ due to the factor of k noted above, but the Hankel spectrum has a tendency to have a spurious peak at $k = 0$ due to the weighting of the zeroth order Bessel function that appears in the formulation. This effect was demonstrated numerically by considering the azimuth averaged spectra and simulations using synthetic signals, and investigated theoretically in terms of the highest phase velocity that can be determined, i.e., the velocity cutoff. For the Hankel spectrum, the problem was to find the minimum k at which a peak can be distinguished from a peak at $k = 0$, while for the wavenumber spectrum the minimum value of k at which a peak can occur is required. The numerical results confirmed and quantified the existence of the bias and the velocity cutoff for the NORESS geometry. The theoretical investigation demonstrated that for both formulations there is a limit that depends only on the array aperture for circular geometries. The numerical and theoretical investigations showed that the wavenumber spectrum is superior to the Hankel spectrum for distinguishing high phase velocities but the Hankel spectrum is more accurate at low phase velocities. Both formulations, however, are asymptotically unbiased for the limit of low phase velocities.

It should be noted that the cutoff is due to the low resolution of the conventional

FK formulation for arrays of limited aperture. To ameliorate or eliminate this problem a number of solutions could be attempted. For waves coming from a single azimuth, the simplest solution is to use the original FK formulation, which exhibits no biases, instead of the wavenumber spectrum. However, the same lack of resolution has limited the usefulness of FK when more than one wavetype or azimuth is present. Another possibility would seem to be an increase in array aperture, but in practice the prospects for seismic waves are considerably limited by loss of coherence of the signal over large intersensor spacings (Ingate *et al.*, 1985). A much more promising solution would seem to be to start from a high-resolution estimate of the FK spectrum, such as the Maximum Likelihood Method (MLM; Capon, 1969). MLM has traditionally been applied to seismic data with great success. In addition to ameliorating the cutoff problem by its high resolution, MLM will also help the sidelobe problem briefly alluded to in the Example but not further discussed. One disadvantage of starting from a MLM formulation of the FK spectrum is that the contour integrals (13) and (14) must be carried out numerically. We will report on the use of MLM in a later publication.

ACKNOWLEDGEMENTS

Much of this research was carried out at the NORSAR/NORESS Data Processing Facility in Kjeller, Norway. The assistance and hospitality of the Director, Dr. Frode Ringdal, is gratefully acknowledged. Dr. Tormod Kværna assisted with the programming and data analysis and Dr. Svein Mykkeltveit gave us much advice about the array. AMD had many discussions with Dr. Eystein Husebye about scattering and the nature of the coda. We would like to thank Steve Taylor, Farid Dowla and George Randall for reviewing the manuscript and making many helpful suggestions. AMD was supported in this research by the Defense Advanced Research Projects Agency through contracts F19628-85-K-0019 (at Georgia Institute of Technology) and F19628-86-K-0004 (at Massachusetts Institute of Technology) administered by the Air Force Geophysics Laboratory. Work performed by DBH was performed under the auspices of the U.S. Department of Energy by the Lawrence Livermore National Laboratory under Contract W-7405-Eng-48. Publication costs have been supported by the Air Force Geophysics Laboratory and by LLNL.

REFERENCES

Bungum, H., S. Mykkeltveit and T. Kværna (1985). Seismic noise in Fennoscandia, with emphasis on high frequencies. *Bull. Seis. Soc. Am. 75*, 1489–1513.

Capon, J. (1969). High-resolution frequency-wavenumber spectrum analysis. *Proc. IEEE 57*, 1408–1418.

Capon, J., R. J. Greenfield and R. T. Lacoss (1969). Long-period signal processing results for the Large Aperture Seismic Array. *Geophysics 34*, 305–329.

Dainty, A. M. (1988). Studies of coda using array and three-component processing. *PA-GEOPH*, in press.

Haubrich, R. A., and K. McCamy (1969). Microseisms: coastal and pelagic sources. *Rev. Geophys. 7*, 539–571.

Ingate, S. F., E. S. Husebye and A. Christoffersson (1985). Regional arrays and processing schemes. *Bull. Seis. Soc. Am. 75*, 1155–1177.

Iyer, H. M., and J. H. Healy (1972). Evidence for the existence of locally-generated body waves in the short-period noise at the Large Aperture Seismic Array, Montana. *Bull. Seis. Soc. Am. 62*, 13–29.

Lacoss, R. T., E. J. Kelly and M. N. Toksöz (1969). Estimation of seismic noise structure using arrays. *Geophysics 34*, 21–38.

Nawab, S. H., F. U. Dowla and R. T. Lacoss (1985). Direction determination of wideband

signals. *IEEE Trans. ASSP-88*, 1114-1122.

APPENDIX

In this Appendix we examine the question of estimation cutoffs analytically starting from (30). For the Hankel spectrum the numerical calculations presented in the text seemed to show that below a certain limit (cutoff) in the true wavenumber K' (or k') the Hankel spectrum always seemed to indicate a wavenumber of 0. We argue the existence of the limit by showing analytically that for sufficiently small k', $\langle \overline{H}(k) \rangle$ is always maximum at the origin. Now:

$$\langle \overline{H}(k) \rangle = E \sum_{m=1}^{M} \sum_{n=1}^{M} J_0(k' \rho_{mn})\, J_0(k \rho_{mn}) \qquad \text{(A-1)}$$

$$\leq E \sum_{m=1}^{M} \sum_{n=1}^{M} |J_0(k' \rho_{mn})|\, |J_0(k \rho_{mn})| \qquad \text{(A-2)}$$

$J_0(x)$ is maximum at the origin and is a monotonically decreasing function in the interval $[0, \alpha]$, where $\alpha \approx 2.40$ is the first zero of $J_0(x)$. The intersensor distances ρ_{mn} are bounded by the array aperture Δ:

$$\rho_{mn} \leq \Delta \qquad \text{(A - 3)}$$

If we choose

$$k' \Delta < \alpha \qquad \text{(A - 4)}$$

then

$$J_0(k' \rho_{mn}) \geq J_0(k' \Delta) > 0. \qquad \text{(A - 5)}$$

Thus, we have:

$$\langle \overline{H}(k) \rangle \quad \leq \quad E \sum_{m=1}^{M} \sum_{n=1}^{M} J_0(k^* \rho_{mn}) \; |J_0(k \rho_{mn})| \qquad \text{(A-6)}$$

$$\leq \quad E \sum_{m=1}^{M} \sum_{n=1}^{M} J_0(k^* \rho_{mn}) \quad = \quad \langle \overline{H}(0) \rangle \qquad \text{(A-7)}$$

which is the desired result. This result demonstrates that the cutoff phenomenon is dependent on aperture: for any $k^* < \alpha/\Delta$, the estimated wavenumber will be 0. The Hankel spectrum cannot distinguish small non-zero wavenumbers from zero wavenumber.

The cutoff phenomenon is slightly more complicated to establish for the wavenumber spectrum. In this case we show that the spectrum cannot have a peak below a certain cutoff wavenumber, k_{min}. We establish that:

$$\frac{d}{dk} \langle \overline{P}(k) \rangle \quad > \quad 0 \qquad \text{for } k < k_{min} \qquad \text{(A-8)}$$

Now:

$$\frac{d}{dk} \langle \overline{P}(k) \rangle \quad = \quad E \sum_{m=1}^{M} \sum_{n=1}^{M} J_0(k^* \rho_{mn}) \; (J_0(k \rho_{mn}) \; - \; k \rho_{mn} \, J_1(k \rho_{mn})) \qquad \text{(A-9)}$$

Again, the first zero of $J_0(x)$ occurs at α, and the first zero of $J_0(x) - x J_1(x)$ occurs at $\beta \approx 1.2$. For x smaller than the appropriate value, both terms are positive. If we choose

$$k^* \Delta \quad < \quad \alpha \qquad \text{(A-10)}$$

then the derivative is positive for all k satisfying

$$k \rho_{mn} \quad \leq \quad k \Delta \quad < \quad \beta \qquad \text{(A-11)}$$

which indicates no peaks for k in the range $[0, \beta/\Delta]$.

FIGURE CAPTIONS

Figure 1. Map of NORESS array seismometer sites. Array center is at 60.7353°N, 11.5414°E.

Figure 2. Teleseismic event recorded at the center seismometer, NORESS. Solid vertical lines delineate analysis window around first P, dashed lines indicate coda windows. Event is a suspected nuclear test at the East Kazakh test site on February 10 1985.

Figure 3. FK spectra of the event shown in Figure 2 at a frequency of 1.6 Hz. (Top) Five second window around first P. (Bottom) Window between 20 and 100 seconds after first P (coda), calculated as average of non-overlapping 5 second windows. From Dainty (1988).

Figure 4. Hankel spectra of the event shown in Figure 2 at a frequency of 1.8 Hz. Windows as for Figure 3.

Figure 5. Wavenumber spectra of the event shown in Figure 2 at a frequency of 1.8 Hz. Windows as for Figure 3.

Figure 6. Linear wavenumber estimated from average Hankel and wavenumber spectra maxima by (30) plotted against true linear wavenumber (solid lines). Long dashed line is Estimated Wavenumber = True Wavenumber. Symbols are results from simulations such as those shown in Figure 7: inverted triangles are for a dominant frequency of 1 Hz and crosses are for a dominant frequency of 2 Hz. Arrows show positions of theoretical wavenumber limits implied by (32) for the Hankel spectrum on the true wavenumber axis, and by (33) for the wavenumber spectrum on the estimated wavenumber axis.

Figure 7. Hankel and wavenumber spectra for a synthetic plane wave signal of phase velocity 23 km/s, azimuth due North and dominant frequency 2 Hz placed on the sensors of the NORESS array. Ordinate is linear wavenumber.

Figure 8. Results shown in Figure 6 replotted as estimated velocity against true velocity for frequencies of 1 Hz (solid lines) and 2 Hz (short dash lines). Long dash line is Estimated Velocity = True Velocity. Symbols as for Figure 6.

Figure 9. FK spectrum for a pure plane wave incident on the NORESS array from the North with a linear wavenumber of 0.1 cycles/km. Dashed circles represent contours of integration in (13) and (14). See text for discussion.

Figure 10. Results of Figure 6 replotted as fractional velocity bias (37) against $K \cdot \Delta = \Delta/\lambda$. Symbols as for Figure 6.

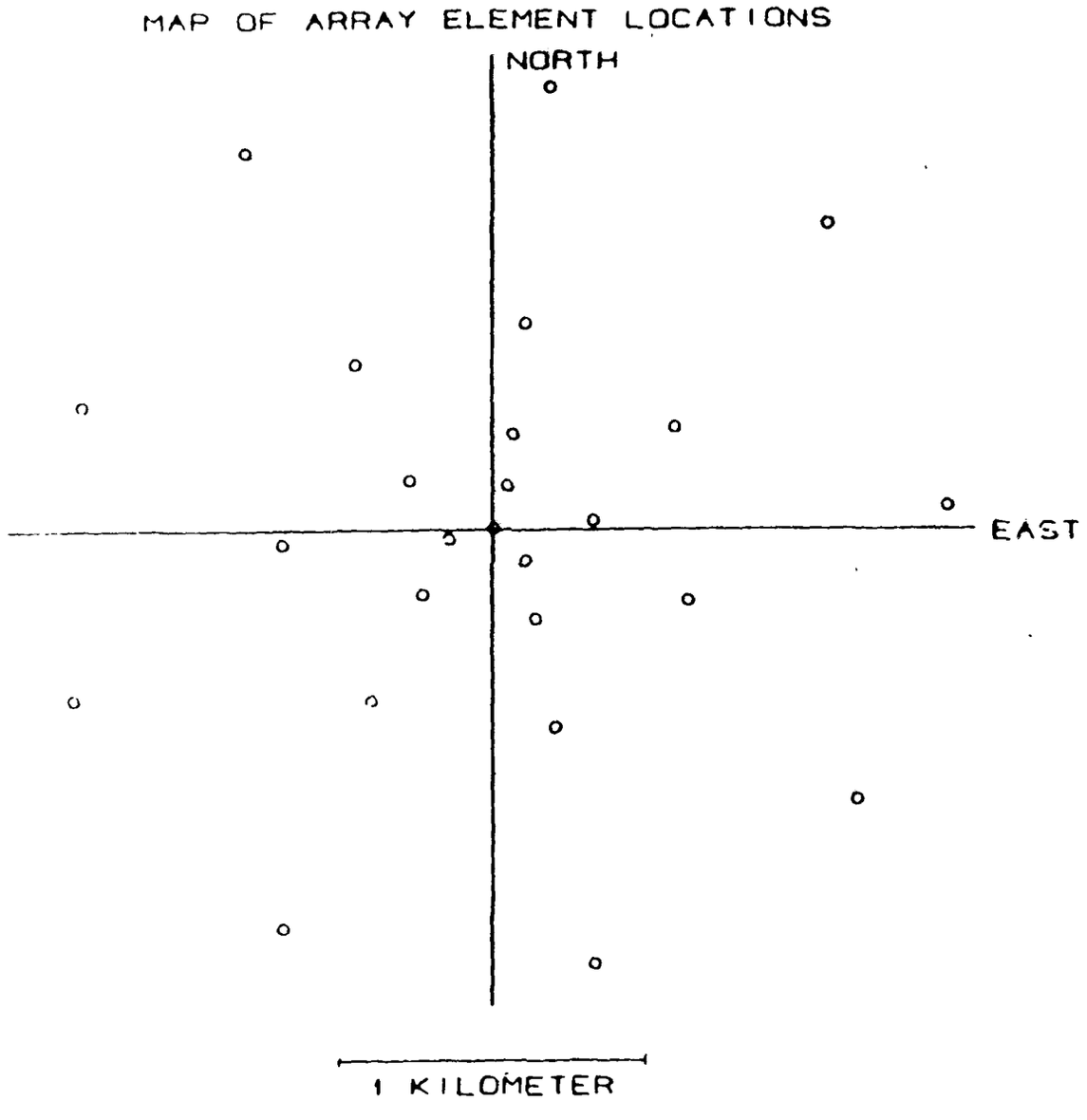

Figure 1

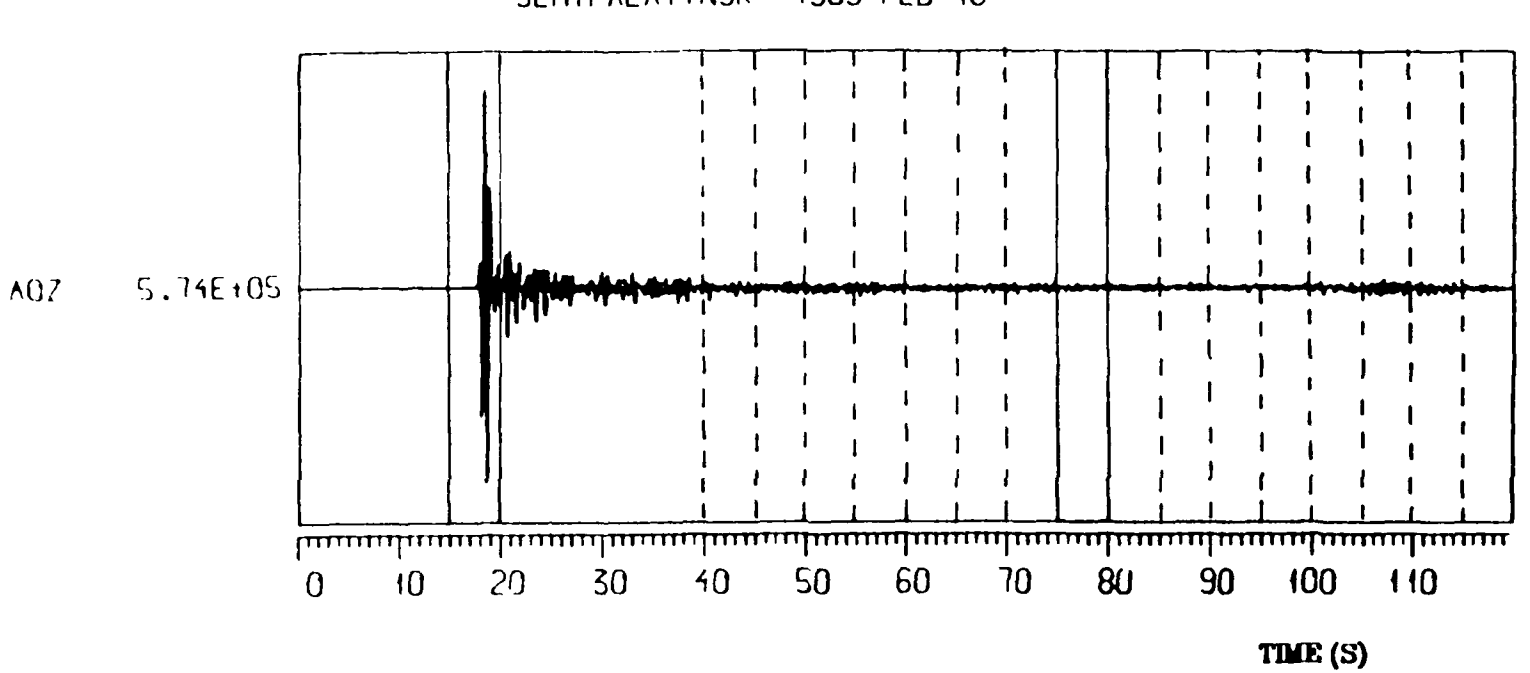
SEMIPALATINSK 1985 FEB 10
A07 5.74E+05
0 10 20 30 40 50 60 70 80 90 100 110
TIME (S)

Figure 2

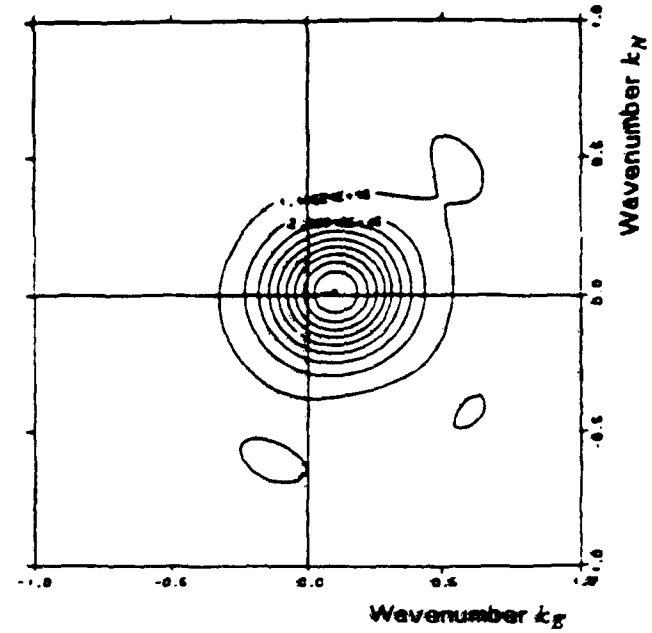

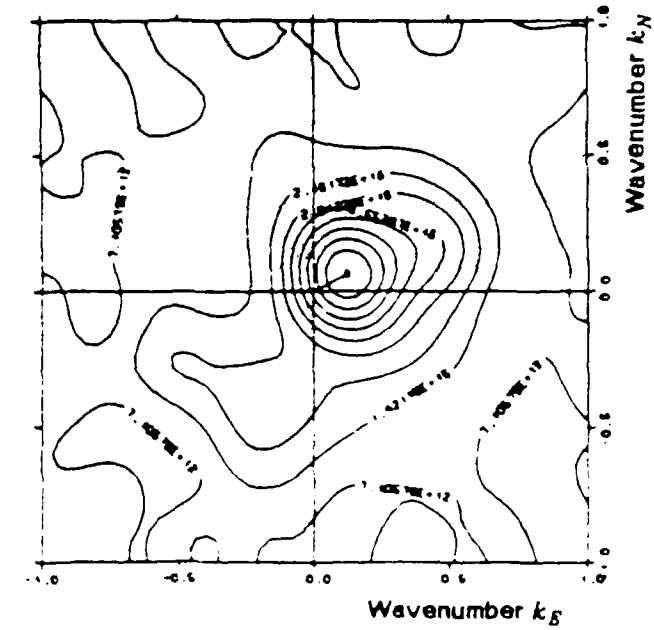

Figure 3

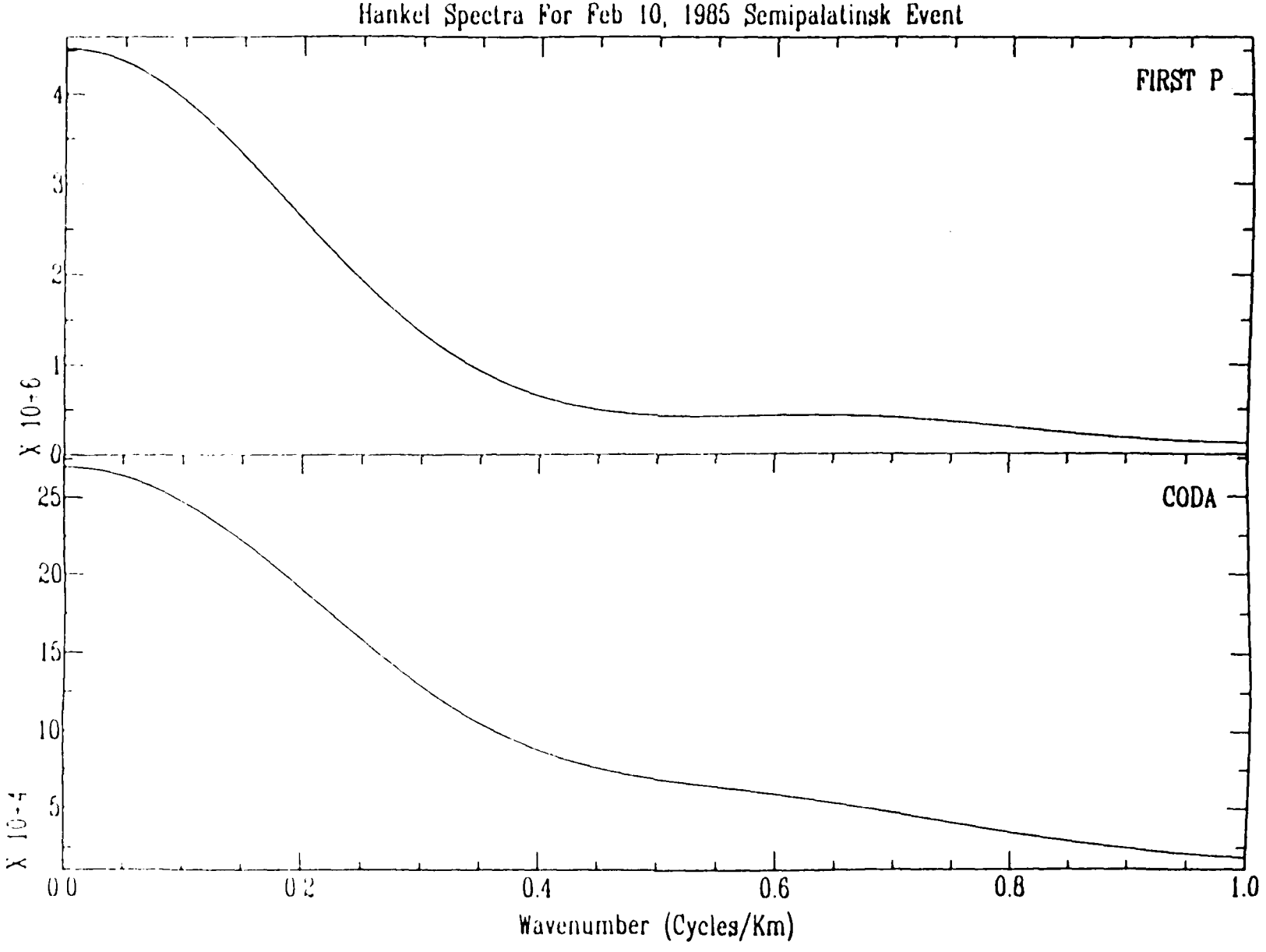
Hankel Spectra For Feb 10, 1985 Semipalatinsk Event
FIRST P
X 10-6
4
3
2
1
0
CODA
X 10-4
25
20
15
10
5
0.0
0.2
0.4
0.6
0.8
1.0
Wavenumber (Cycles/Km)

Figure 4

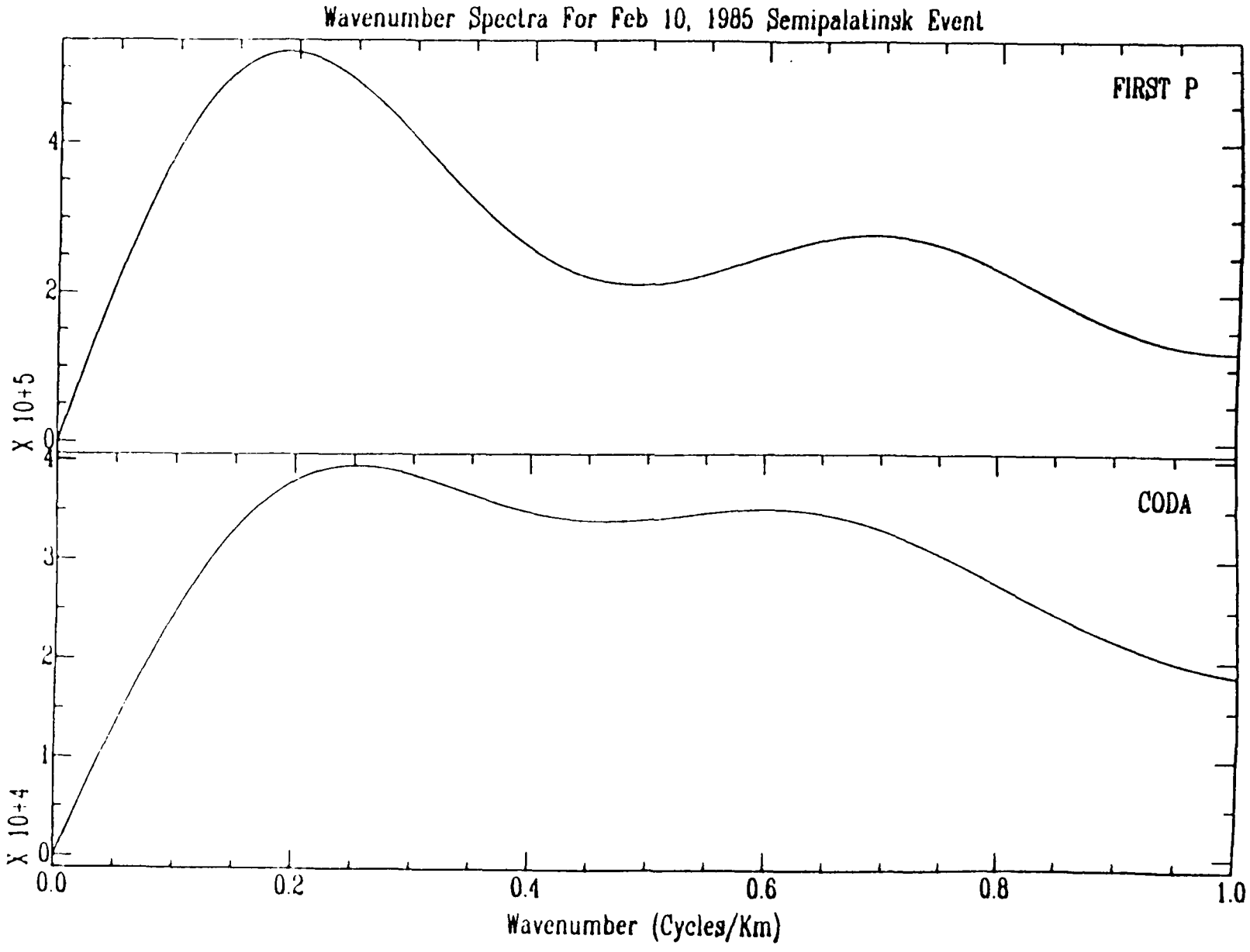
Wavenumber Spectra For Feb 10, 1985 Semipalatinsk Event
FIRST P
CODA
X 10+5
X 10+4
0
2
4
1
3
0.0
0.2
0.4
0.6
0.8
1.0
Wavenumber (Cycles/Km)

Figure 5

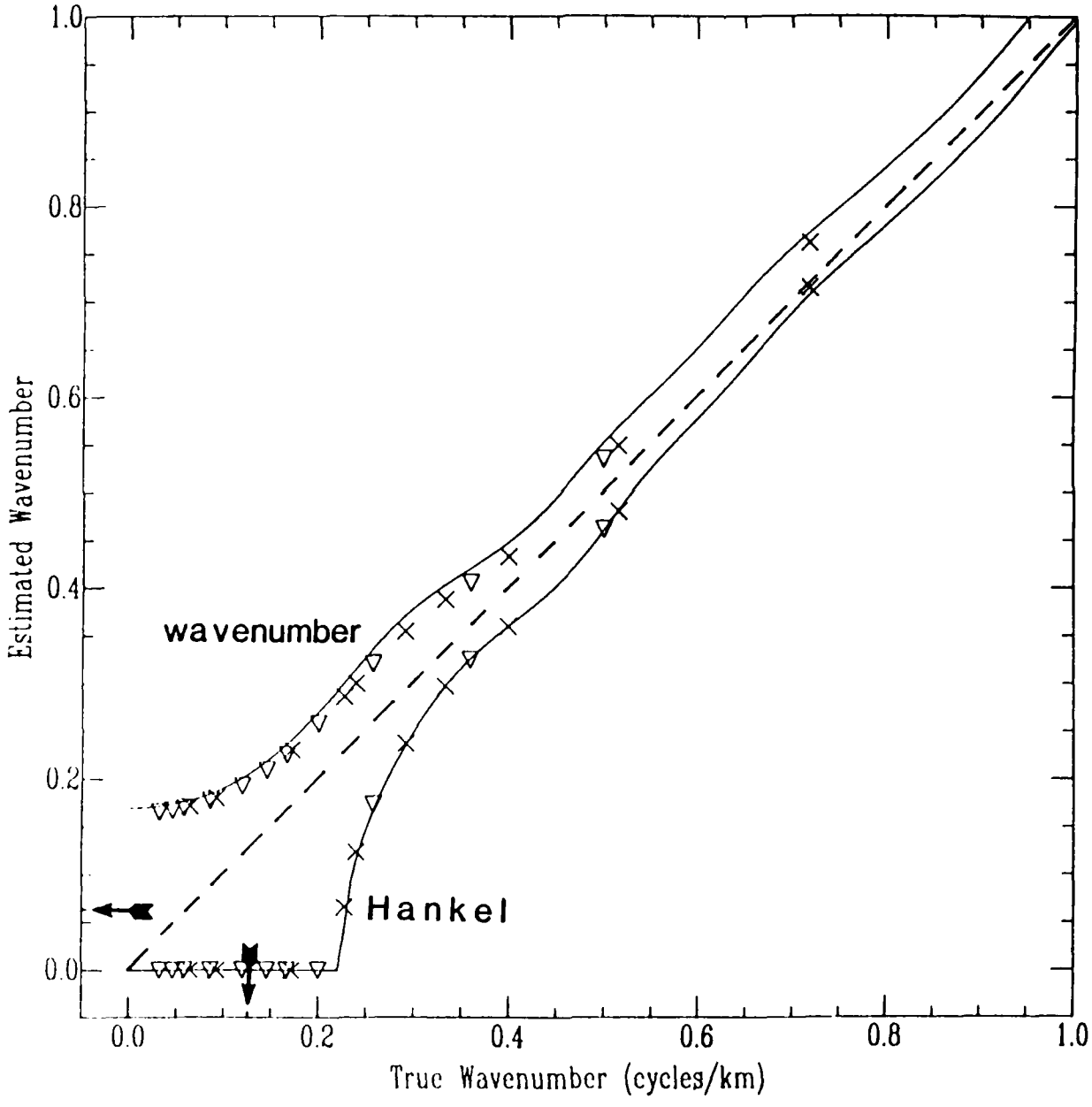
1.0
0.8
0.6
0.4
0.2
0.0
Estimated Wavenumber
wavenumber
Hankel
0.0
0.2
0.4
0.6
0.8
1.0
True Wavenumber (cycles/km)

Figure 6

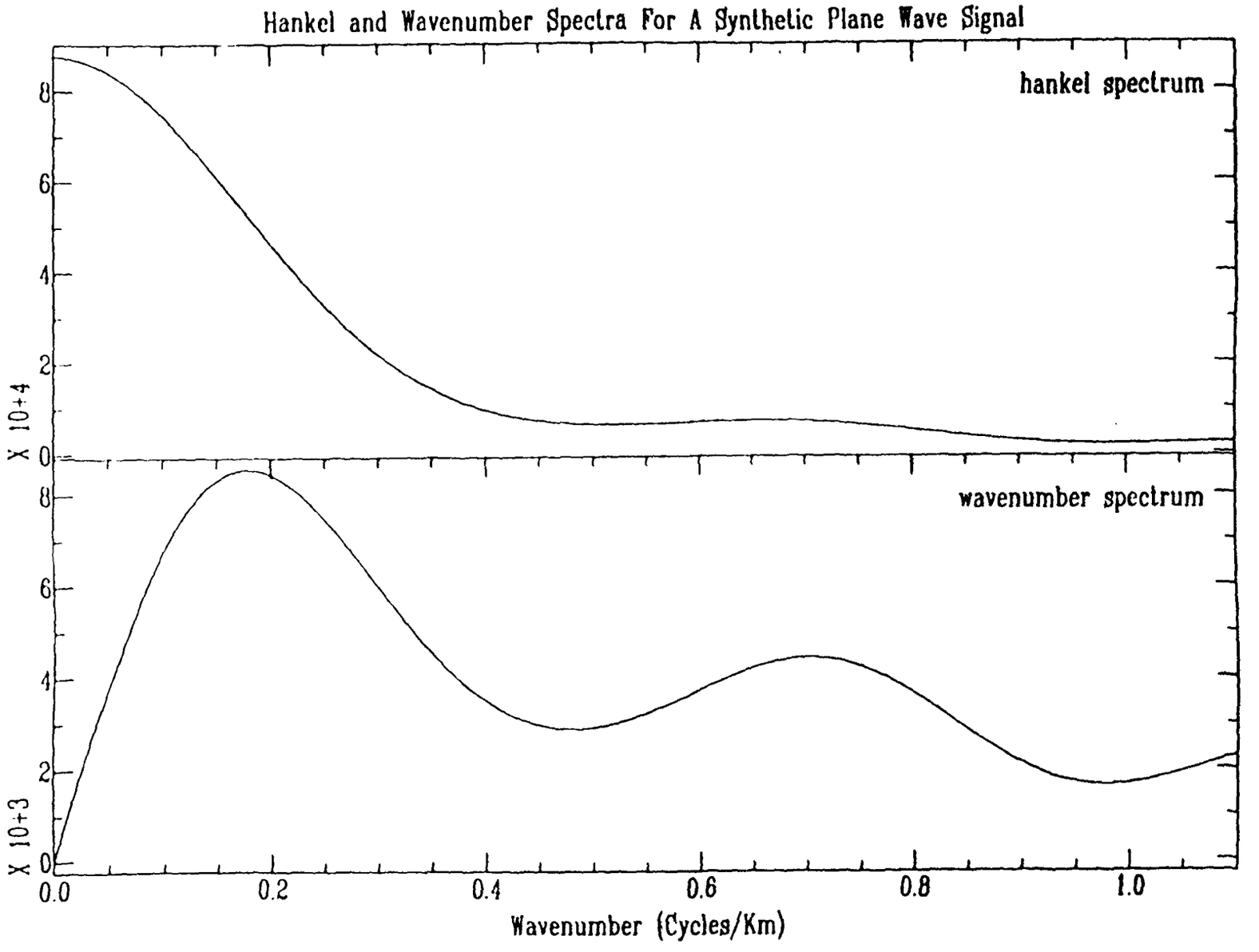
Hankel and Wavenumber Spectra For A Synthetic Plane Wave Signal
hankel spectrum
wavenumber spectrum
X 10+4
X 10+3
0
2
4
6
8
0.0
0.2
0.4
0.6
0.8
1.0
Wavenumber (Cycles/Km)

Figure 7

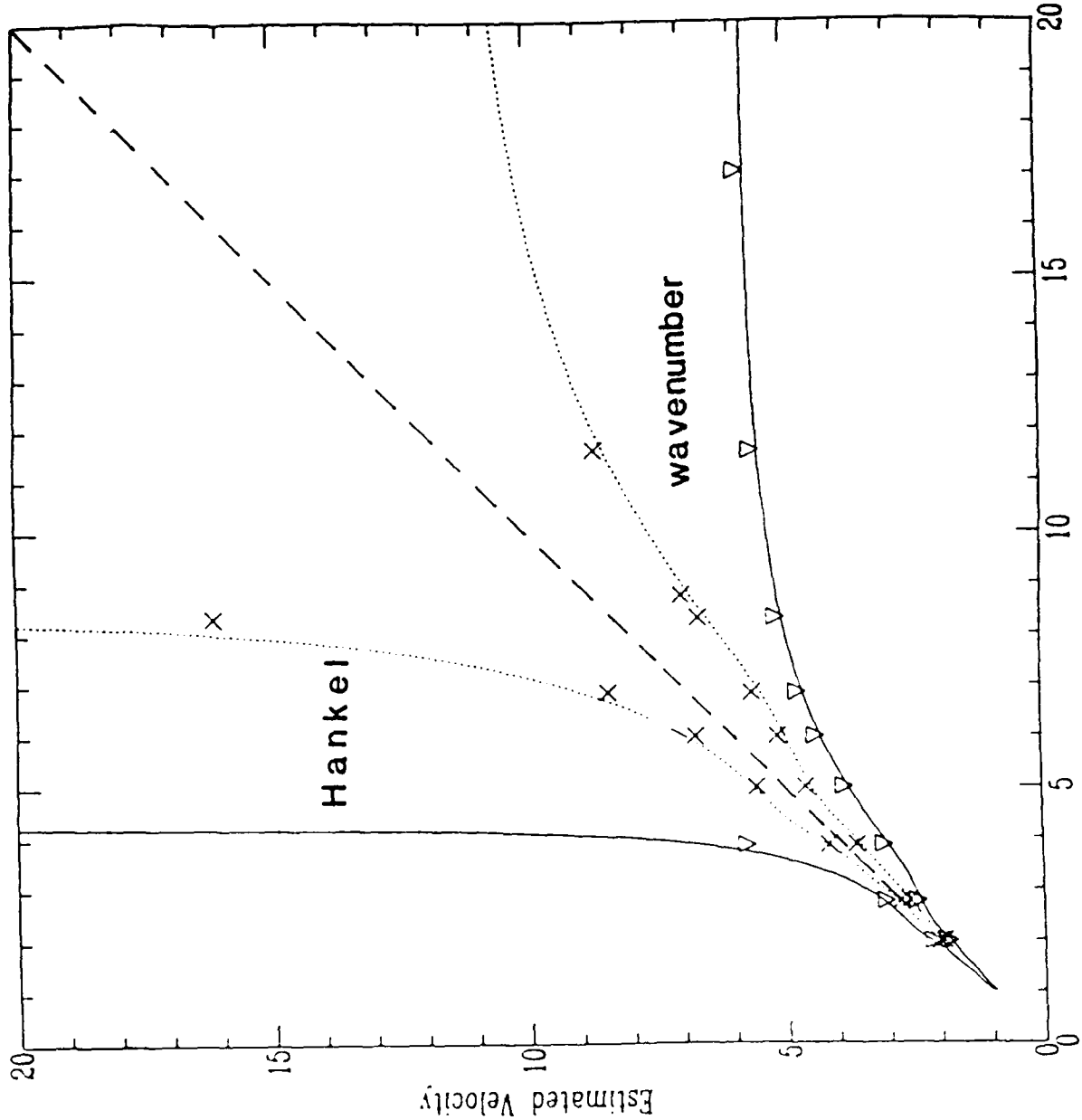
Hankel
wavenumber
Estimated Velocity
True Velocity (km/sec)
0
5
10
15
20

Figure 8

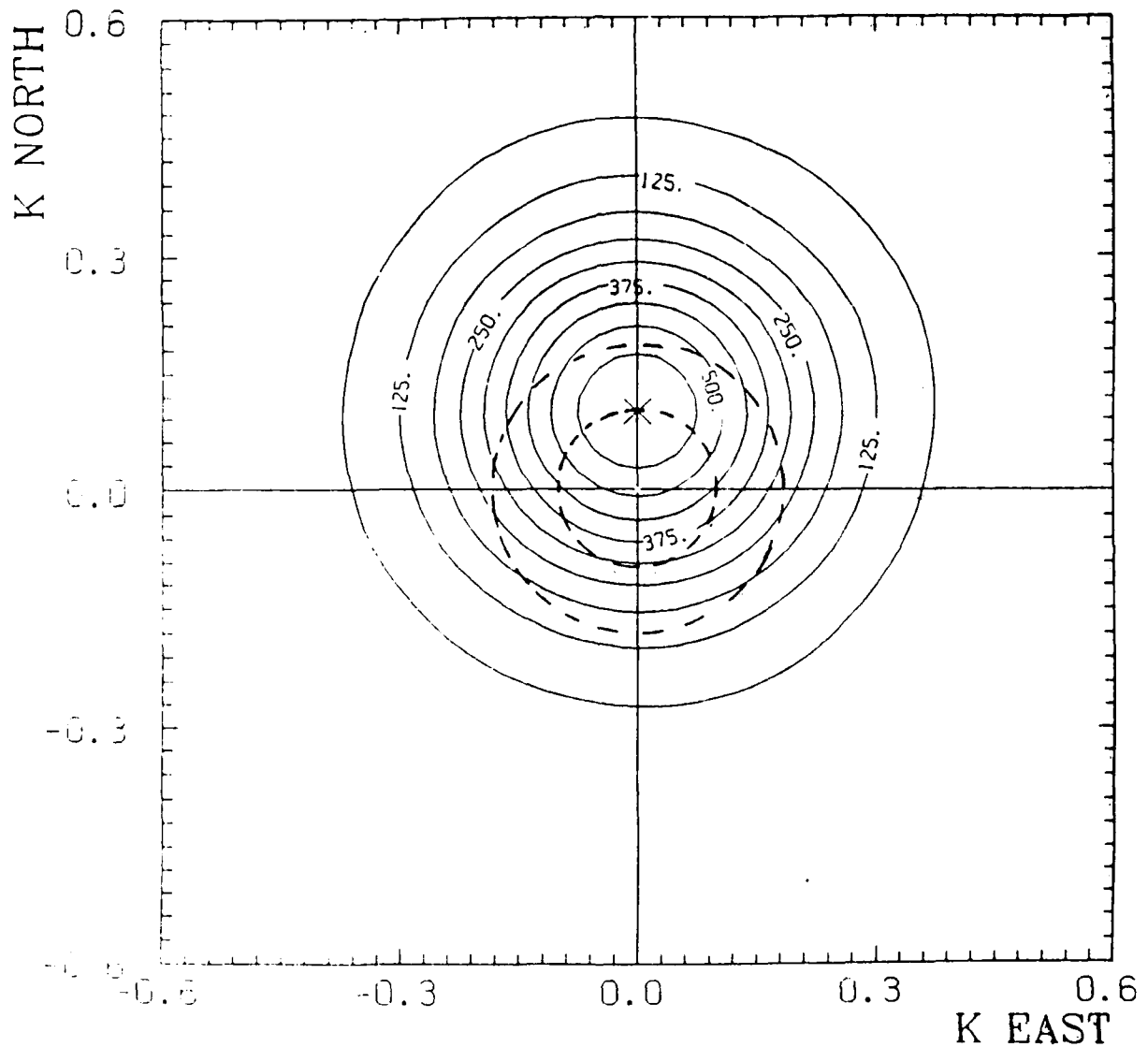

Figure 9

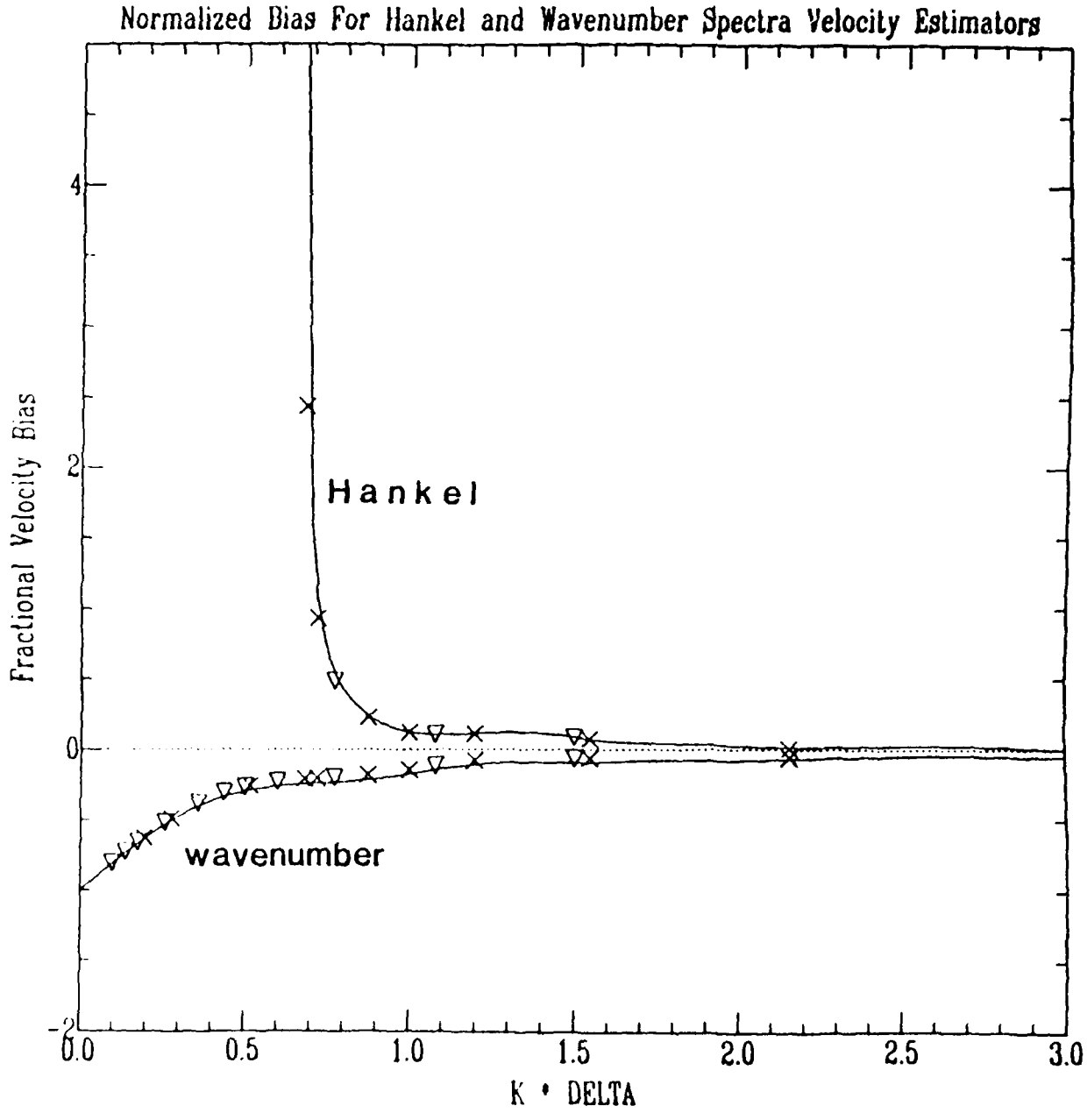
Normalized Bias For Hankel and Wavenumber Spectra Velocity Estimators
Fractional Velocity Bias
4
2
0
-2
Hankel
wavenumber
0.0
0.5
1.0
1.5
2.0
2.5
3.0
K • DELTA

Figure 10

A MODEL FOR ATTENUATION AND SCATTERING IN THE EARTH'S CRUST

M. Nafi Toksöz, Anton M. Dainty*, Edmund Reiter
Earth Resources Laboratory
Dept. Earth, Atmospheric, and Planetary Sciences
Massachusetts Institute of Technology
Cambridge MA 02138
U. S. A.

and

Ru-Shan Wu
Physics and Inst. of Tectonics
University of California
Santa Cruz CA 95064
U. S. A.

In press, PAGEOPH
1988

*Also at:
Air Force Geophysics Laboratory/LWH
Hanscom AFB MA 01731
U. S. A.

Abstract

The mechanisms contributing to the attenuation of earthquake ground motion in the distance range of 10 to 200 km are studied with the aid of laboratory data, coda waves, Rg attenuation, strong motion attenuation measurements in the northeast United States and Canada, and theoretical models. The frequency range 1–10 Hz has been studied. The relative contributions to attenuation of anelasticity of crustal rocks (constant Q), fluid flow and scattering are evaluated. Scattering is found to be strong with an albedo $B_0 = 0.8$–0.9 and a scattering extinction length of 17–32 km. The albedo is defined as the ratio of the total extinction length to the scattering extinction length. The Rg results indicate that Q increases with depth in the upper kilometer or two of the crust, at least in New England. Coda Q appears to be equivalent to intrinsic (anelastic) Q and indicates that this Q increases with frequency as $Q = Q_0 f^n$, where n is in the range 0.2–0.9. The intrinsic attenuation in the crust can be explained by a high constant Q ($500 \leq Q_0 \leq 2000$) and a frequency dependent mechanism most likely due to fluid effects in rocks and cracks. A fluid-flow attenuation model gives a frequency dependence ($Q \simeq Q_0 f^{0.5}$) similar to those determined from the analysis of coda waves of regional seismograms. Q is low near the surface and high in the body of the crust.

Introduction

The dependence of ground motion U of frequency ω with distance r from the source has been described by the equation

$$U(r,\omega) = S(\omega) \cdot F(r) \cdot \exp[-r\omega/(2Qv)] \tag{1}$$

In (1) S represents the source and v is the seismic wave velocity. The factor $F(r)$ is the geometrical spreading factor due to the propagation of motion in a perfectly elastic medium without random scattering. In a homogeneous medium $F(r) = 1/r$ for body waves and $= 1/\sqrt{r}$ for surface waves (not including the effect of dispersion), and this form is often used at ranges of less than 100 km. The exponential term parameterised by Q describes the effect of attenuation due to imperfect elasticity (anelastic attenuation) and random scattering. However, a recently developed theory of wave scattering in absorbing and heterogeneous media (Wu 1984, 1985) indicates that the spectral intensity of ground motion varies with distance in a much more complicated manner when multiple scattering is considered. In this theory, the shape of the intensity-distance curve is controlled by the seismic albedo B_0 of the medium discussed below, as shown in Figure 1. Only for the case of $B_0 \ll 0.5$ can the curve be approximately expressed in a simple exponential form after geometric spreading corrections. Our objective is to examine the relative contribution of scattering and anelastic attenuation in the crust and to propose a general crustal model of attenuation and scattering.

While physical definitions of Q are given in the literature in practice Q is usually measured by methods based on equation (1) or the corresponding time equation. A difficulty that arises with this 'operational' definition of Q is that different results may be obtained based on different

methods of measurement even in simple cases (Aki and Richards, 1980, p. 168). A particularly important case is the influence of scattering. Without scattering, the Q measured using (1) will represent solely anelastic attenuation. However, if a short pulse travels through a medium in which both scattering and anelasticity occur, then the total Q, Q_t, is (Dainty, 1981)

$$1/Q_t = 1/Q_a + 1/Q_s \tag{2}$$

In (2) Q_a is the anelastic Q. The loss of energy from the pulse due to scattering is described by $Q_s = \omega/(2\eta_s v)$, where η_s is the scattering coefficient discussed below. Equation (2) indicates that for the case of a short pulse the influence of anelastic attenuation and scattering cannot be separated unless some model for the Q components is used. However, the scattered energy represented by Q_s is merely deflected, not lost from the wavefield. Measurements of Q which examine a substantial window in time of the seismogram, such as coda Q, may include some of this energy.

Below we present summaries of three investigations that measure Q in different ways. The first interprets the attenuation of strong motion measurements using pseudo velocity. Since an integration over the duration of strong motion is carried out in this measure, the total energy in the seismogram including scattered energy is measured. Our investigation explicitly examines the question of the relative attenuation due to anelasticity and scattering and separates the contribution of each using transport theory. The second investigation examines the Rg phase (fundamental mode Rayleigh wave) in the frequency range 1–10 Hz at distances of 10–30 km. This is a pulse measurement and equation (2) should apply, i. e., the total Q represents the combined effect of anelasticity and scattering without separating them. Finally we discuss the implications of some previous measurements of coda Q. While this method has become a standard method of measuring

Q, the interpretation of the results has not been clear.

We consider primarily attenuation in the distance range of 10 to 100 km. This interval is ideal for several important reasons. At distances shorter than about 10 km from the source, non-linear behavior of materials due to high strains ($\epsilon \geq 10^{-5}$) can dominate. At distances greater than 100 km, the geometric spreading effects, due to velocity-depth functions and multiple branches of travel-time curves, become site-specific and uncertain. Another important factor for favoring this distance range is that a considerable amount of new attenuation data has been obtained both from strong motion records and the analysis of seismic coda waves. Also, because of the rapid attenuation of high frequency Rg it is only easily observed in this distance range.

Before reviewing the attenuation data, it is important to define the terminology. The attenuation for a given wave type (P or S) is defined as the inverse of the quality factor Q, and related to other measures by:

$$\frac{1}{Q} = \frac{\alpha v}{\pi f} = \frac{\delta}{\pi} \tag{3}$$

where α is the anelastic attenuation coefficient, v the wave velocity, f the frequency, and δ the logarithmic decrement.

Attenuation Q^{-1} or the quality factor Q are dimensionless quantities. Physically,Q^{-1} is equal to the ratio of energy dissipated per cycle to the total energy. For small attenuation, (i.e. $Q^{-1} \leq 0.1$), additional relationships can be established in terms of stress-strain relationships:

$$\frac{1}{Q} = \frac{M_I}{M_R} = \tan\phi \simeq \phi \tag{4}$$

where M_I and M_R are the imaginary and real parts of the appropriate elastic modulus ($M = M_R + iM_I$) and ϕ is the phase lag of the strain behind the stress (i.e., loss tangent). The dimension

of the anelastic attenuation coefficient α is generally given as dB/unit length or nepers per unit length. The relationship between the two is α(dB/unit length) = 8.686 α(nepers/unit length).

Most of the data for crustal attenuation comes from coda waves (Aki and Chouet, 1975; Aki, 1980; Pulli, 1984; Singh and Herrmann, 1983; Singh, 1985; Gupta et al., 1983; Rautian and Khalturin, 1978; Roecker et al., 1982; Herrmann, 1980). These measurements generally give attenuation that decreases with frequency in the frequency range of f =0.5 to 25 Hz. A typical result for New England is $Q_c(f) = 460f^{0.4}$ (Pulli, 1984). The increase of Q with frequency and the high values ($Q \geq 1000$) at frequencies above 10 Hz in the Eastern United States cannot be reconciled with the laboratory measurements of Q in crustal rocks (see Toksöz and Johnston, 1981 for a comprehensive compilation). Most laboratory data suggest that, at least for dry rocks, Q is independent of frequency (Birch and Bancroft, 1938; Peselnick and Outerbridge, 1961; Klima et al., 1964; Knopoff, 1964; Pandit and Savage, 1973; Toksöz et al., 1979; Nur and Winkler, 1980; Johnston and Toksöz, 1980; Tittman et al., 1981). Water saturation generally decreases Q values of both P and S waves, although the decrease is much greater for S-waves than for P-waves.

In the laboratory Q increases with increasing confining pressure. However, the laboratory Q values at pressures of 2 kilobars or more in crystalline rocks are generally less than 1000 (Klima et al., 1964; Bradley and Fort, 1966; Mason et al., 1970). It is only in the case of totally outgassed and volatile free rocks that Q values of 2000 or more have been obtained (Clark et al., 1980; Tittman et al., 1974).These values have been observed in the completely dry environment of the moon (Dainty et al., 1976). The Earth's crust is not free of water and volatiles and the high Q values cannot be attributed to dehydration. Thus the high Q values need to be explained.

Although Q is independent of frequency in dry rocks, it may be frequency dependent in saturated and partially saturated rocks (Gardner et al., 1964; Winkler and Nur, 1979; Spencer, 1981; Tittman et al., 1981; Toksöz et al, 1979). The saturation may produce relaxation peaks at certain frequencies and increase and decrease of Q on two sides of a peak. A question we wish to investigate is whether such relaxation phenomena and fluid motions can explain the frequency dependence of crustal Q values measured from coda waves.

Interpretation of Strong Motion Data

Scattering of elastic waves propagating in a heterogeneous medium contributes to the attenuation of these waves. Scattering attenuation is not an energy dissipation mechanism, but only an energy redistribution in space and time, therefore, it is a geometric effect. Under the single scattering approximation, the scattering attenuation cannot be separated from the intrinsic attenuation. In order to separate these two attenuation mechanisms, we need to use the multiple scattering theory. There is no general solution for the multiple scattering theory. However, several special cases have been studied (O'Doherty and Anstey, 1971; Kopnichev, 1977; Dainty and Toksöz, 1977, 1981; Richards and Menke, 1983; and Gao et al., 1983a, b). Wu (1984, 1985) formulated the multiple scattering problem in the frequency domain using radiative transfer theory. In the case of isotropic scattering with a point source in an infinite random medium, an exact solution can be obtained (Appendix A).

Figure 1 shows the distribution of seismic wave energy with distance calculated by the theory. In the figure, the distance is normalized by the extinction length L_e, which is the reciprocal of the

extinction coefficient η_e:

$$\begin{aligned} L_e &= 1/\eta_e \\ \eta_e &= \eta_a + \eta_s \end{aligned} \tag{5}$$

where η_a is the energy absorption coefficient due to anelasticity of the medium and η_s is the scattering coefficient which is defined as the total scattered power by a unit volume of random medium per unit incident power flux density. Note that η_a is related to the anelastic attenuation coefficient given in equation (3) by $\eta_a = 2\alpha$. In Figure 1 the curve shapes change depending on the seismic albedo B_0 of the medium, which is defined as:

$$B_0 = \frac{\eta_s}{\eta_e} = \frac{\eta_s}{\eta_s + \eta_a} \tag{6}$$

For the case of large albedo ($B_0 > 0.5$), i.e. when the medium is strongly heterogeneous, and scattering is significant, the curves are of arch shape. The maxima of the curves depend on the extinction coefficient ($\eta_e = \eta_s + \eta_a$). Therefore it is possible to obtain B_0 and η_e from the energy density-distance curves, and thus separate the scattering effect from the intrinsic attenuation.

The theory has been applied to local earthquakes in Hindu Kush region (Wu, 1984; Wu and Aki, 1987) with the conclusion that the scattering attenuation in that region is not the dominant factor ($B_0 \leq 0.5$). In this study, we look at the attenuation data in the eastern United States where anelastic attenuation may be low.

Figures 2a and 2b are the strong motion data (pseudo velocity) in Northeastern America for the case of $f = 5$ Hz and 1 Hz respectively (with 5% damping). The solid lines in the figures are the best fits to the data. If we assume that the received strong motions are composed of both the direct arrivals and the scattered waves, then we can compare curves given in Figure 2 with the

Table 1: Medium parameters at f=1 and f=5 Hz based on multiple scattering theory

Parameter	f =1 Hz	f = 5 Hz
L_e	15 km	25 km
B_0	0.9	0.8
η_s	0.06 km^{-1}	0.03 km^{-1}
$L_s(=1/\eta_s)$	16.7 km	31.3 km
η_a	0.0067 km^{-1}	0.0081 km^{-1}
$L_a(=1/\eta_a)$	150 km	125 km
$Q_s(=kL_s)$	30	280
$Q_a(=kL_a)$	270	1120

data to obtain the seismic albedo B_0 and the intrinsic quality factor Q_a. In Figure 3, the PSV data are corrected for the geometric spreading ($1/r$ for body waves) and then squared to compare with the theoretical predictions. The best theoretical curves are also drawn in the Figure. We can see that in the first 100 km the fit between theory and data is generally good except for a few points which are very close to the source. For greater distances, the data gradually deviate from the theory and become flatter. This may be due to the dominance of Lg waves at great distances. The discrepancy of data and theory at very close distances is probably due to the non-linear effects. From these comparisons of data with theory, we obtain the average seismic albedo $B_0 = 0.9$ and the extinction length $L_e = 15$ km for 1 Hz waves and $B_0 = 0.8$, $L_e = 25$ km for 5 Hz waves. The medium parameters based on these values are listed in Table 1.

In Figure 4 we plot the theoretical curves of the PSV-distance relation for different seismic albedo B_0 when the extinction length is fixed at 15 km. A smaller albedo means a smaller intrinsic

Q and therefore has a steep decrease of amplitude with distance. Figure 5 shows different curves of different albedos when the intrinsic Q is fixed at $Q_a = 1350$. We can see that the strong scattering will make the apparent attenuation much bigger than the intrinsic attenuation when the distance is larger than the absorption extinction length, L_a. However, the amplitude change is not exponential for small distances.

Results given in Table 1 give a good fit to the data with a consistent set of parameters at $f =$ 1 Hz and $f = 5$ Hz. They suggest a frequency dependent anelastic $Q_a = 270f^{0.88}$. As discussed in the first section while reviewing the laboratory data, such variation of Q with frequency cannot be explained without a relaxation mechanism. In the crust, the fluids may provide such a mechanism.

Attenuation of Rg

The data set used consists of recordings of blasts for a refraction experiment in southeastern Maine conducted by the USGS (Doll et al., 1986). The largest phase from these near surface sources, and hence the phase with the peak amplitude, is Rg, the fundamental mode Rayleigh wave. Some examples of the seismograms are shown in Figure 6. The attenuation of Rg can provide useful information first, because it shows the affect of the attenuation mechanisms on an isolated, relatively short pulse, and second, it gives information about the depth dependence of Q from the frequency dependence. The frequencies observed on the records for Rg are 1–10 Hz. To calculate Q, equation (1) is rewritten for Rg in terms of the attenuation coefficient $\gamma(\omega)$ as

$$\ln(\sqrt{r}U(r,\omega)) = \ln S(\omega) - r \cdot \gamma(\omega) \tag{7}$$

A windowed portion of seismograms at different ranges r from a single shot is Fourier transformed to find $U(r,\omega)$. Since the spectrum window contains the entire Rg wave train, there is no correction for dispersion. The source term $S(\omega)$ is common to all seismograms. Accordingly, the slope of a least square fit straight line to the left side of (7) will determine γ. The total Q_t in the sense of equation (2) may be calculated from $Q_t = \omega/(2\gamma v)$. Note that we distinguish the experimentally determined attenuation coefficient γ' from the anelastic attenuation coefficient α in equation (3), since the two are not in general equal by equation (2).

In Figure 7 we show average Q for the area together with models and fits to the data under three different assumptions concerning the frequency dependence of Q. Discussing the measured values first, all Q values are less than 50, and this indicates strong attenuation in the uppermost crust. The Rg Q values are substantially lower than those derived by Pulli (1984) from coda discussed below and have a different frequency dependence: Pulli obtained a Q of 460 at 1 Hz, increasing with frequency. It should be noted that at all frequencies the coda results are probably averages for the whole crust while Rg Q is sensitive to near surface Q and has a depth dependence that varies with frequency. While it is not possible to separate Q_t into Q_a and Q_s, the Q_t values are similar to Q_s in the previous section and suggest that scattering is important, although Q_a is probably also low, as discussed below.

Rg Q at any frequency is a weighted average over depth of both compressional and shear Q, but mainly shear Q. This weighting depends on frequency, since the lower the frequency the greater the penetration of the Rg motion. It then becomes difficult to separate frequency variation of Rg Q due to depth dependence from frequency dependence at a given depth. As a first step in attacking

this difficulty, Figure 7 gives results for three different cases in which the frequency dependence of shear Q is fixed at all depths as $Q_k = Q_{0k} f^n$, where k is the layer index of a layered model and $n = 0, 0.5, 1$ respectively, spanning the observed range (Toksöz et al., 1988). In Figure 7 Q_{0k} (i.e., Q at 1 Hz) is plotted as a function of depth with the fit to the observations shown above. The three choices of n can be thought of as representing attenuation due to microcracks and grain boundary sliding ($n = 0$; Toksöz and Johnston, 1981), attenuation due to fluid flow in major open fractures ($n = 0.5$; Toksöz et al., 1987), and attenuation due to scattering ($n = 1$; Dainty, 1981). Other mechanisms of attenuation are also possible, but the three presented here must certainly be examined in the low pressure, highly heterogeneous environment of the upper crust.

For all of the models Q may only be determined down to a depth of about 3 km due to the limited penetration of Rg. From Figure 7, the constant Q model ($n = 0$) has lower Q at depth than near the surface. This contradicts laboratory data and investigations in other regions and we reject this model. For the case $n = 1$ data at high frequencies cannot be fit because of the strong frequency dependence of Q, although a reasonable fit is found below 2 Hz. A better fit is obtained for $n = 0.5$, except below 1.5 Hz.

To extend the attenuation profile deeper into the crust we use Rayleigh wave data from central North America in the period range 4 to 20 sec (Herrmann and Mitchell, 1975; Mitchell, 1980). A Q structure that fits both data sets is shown in Figure 8. In the top 2 km of this model the Q structure is determined by the high frequency ($f \geq 0.85$ Hz) data presented above; the frequency dependence is $Q = Q_0 f^{0.5}$. The deeper Q structure is controlled by the longer period data of Mitchell (1980). To estimate the frequency dependence, we note that the attenuation (Q^{-1}) due to

scattering or fluid flow is peaked at a critical frequency. Below the critical frequency attenuation decreases rapidly with decreasing frequency: Q^{-1} is proportional to f for fluid flow (Toksöz et al., 1987) and to f^2 for scattering (Frankel and Clayton, 1986). The effect is make frequency dependent Q negligably small at low frequency and intrinsic anelasticity dominates. We assume $Q = Q_0$ for $f < 0.85$ Hz in the inversion of the combined data sets.

The final attenuation model has low Q at shallow depth and high Q (¿ 1000) below about 5 km. Constraining the details of the Q profile in the transition zone requires Rg attenuation data for $0.2 < f < 1.0$ Hz.

Coda Q

Since the introduction of the method by Aki and Chouet (1975), measurement of Q from the decay of coda has become a standard technique. There has, however, been some question regarding what has been measured. To help answer this question we have compared our results for strong motion Q to the work of Pulli (1984) on coda Q in New England. Pulli noted that there was an apparent change in the decay rate of the coda at about 100 s after earthquake origin time, leading to different estimates of coda Q, Q_c. Before 100 s

$$Q_c = 140 f^{0.95} \tag{8}$$

where f is frequency, while at times longer than 100 s

$$Q_c = 660 f^{0.4} \tag{9}$$

The average, ignoring the decay rate change, is

$$Q_c = 460 f^{0.4} \tag{10}$$

Note that for all cases Q_c is similar to Q_a previously obtained from the strong motion data and greater than Q_s. The Q_c found for shorter times unquestionably refers to the crust and is closest to the Q_a results for the strong motion data, but may still have some contribution from scattering (Dainty et al., 1987). The longer time results are consistent with the investigation of Singh and Herrman (1983) covering the continental U. S., although it is not clear whether they refer to the crust only or to the whole lithosphere. It is less likely that scattering is included in Q_c at long times. Of particular interest are the frequency exponents $n = 0.95$ and $n = 0.4$. Values close to 0.5 have often been obtained in other studies if Q at 1 Hz (Q_0) is not too high. On the other hand, if Q_0 is high, then the frequency exponent is often low, for example, Singh and Herrman (1983) quote

$$Q_c = 1000 f^{0.2} \tag{11}$$

for the central U. S. In tectonic regions and at short coda times Q_0 is often smaller ($\simeq 100$) and n may range up to 1 (Singh and Herrman, 1983; Herraiz and Espinosa, 1987; Dainty et al., 1987). In this paper we will make the preliminary interpretation that coda Q in stable regions is representative of anelastic Q because of the similarity with the strong motion Q_a noted, and that because coda Q can be measured easily and reliably it gives the best estimate of the frequency dependence of the anelastic Q.

One reason for assuming coda Q is a measure of average crustal Q, at least in some cases, is the similarity of coda Q and Lg Q. Recently Campillo et al. (1985) have demonstrated this in a

detailed study in central France of both Lg Q and Q in the early coda, obtaining for both cases

$$Q = 300f^{0.5} \tag{12}$$

This is not very different from the average result of Pulli (1984).

Model of Crustal Scattering and Attenuation

Our studies of scattering and anelastic attenuation with distance at frequencies of 1–10 Hz indicate that the relative effect of scattering is strong. The result of this is a complex interplay between the type of measurement made and the appropriate attenuation relation. Measurements of quantities such as pulse amplitude will feel the full force of scattering attenuation and will decay rapidly with Q dominated by scattering. Measurements such as coda will decay less rapidly because some of the scattered energy is rescattered back into the measurement window. A crucial parameter in the description of these effects is the albedo, which is the ratio of attenuation due to scattering to total attenuation. In New England we found an albedo of 0.8–0.9, indicating the importance of scattering. This strong scattering means that coda Q is probably most closely identified with anelastic crustal Q, which appears to be frequency dependent. The results from Rg indicate that there is a low Q surface layer about 2 km thick with $Q \leq 100$.

Laboratory data and observations made in boreholes help to achieve an understanding of the physical mechanisms contributing to the attenuation of seismic waves at regional distances. Laboratory measurements of attenuation in "wet" rocks give relatively low intrinsic Q ($Q \leq 200$) even at pressures of 2 kb, and do not indicate that Q values would increase significantly with pressure. A primary mechanism for this attenuation is friction along grain boundaries and microcracks (Walsh,

1966; Toksöz and Johnston, 1981). Recent studies indicate that in "wet" rocks microcracks heal at pressures of about 2 kb and temperatures of 400°C (Smith and Evans, 1984; Rovetta et al., 1987). Thus, microcracks would not contribute to attenuation in the crust below a few kilometers and intrinsic Q below this depth is likely to be high ($Q \geq 1000$).

Data from wells drilled in crystalline rocks shows the presence of both major and minor fractures. The fluid flow in such fractures can contribute significantly to attenuation and give a frequency dependent Q (Toksöz et al., 1987). Above a critical frequency, which could be as low as 1 or 2 Hz, Q is proportional to the square root of frequency ($f^{0.5}$). Below the critical frequency Q is proportional to inverse frequency (f^{-1}). There is an even stronger frequency dependence of attenuation due to scattering with a peak between $f = a/\lambda$ and $f = 2a/\lambda$, where a is the correlation length of random scatterers and λ is the wavelength of seismic waves. Above and below this peak Q is proportional to frequency (f^1) and inverse frequency squared (f^{-2}) respectively (Wu, 1982; Dainty, 1984; Frankel and Clayton, 1986).

With all these mechanisms included, a conceptual attenuation and scattering model for the crust can be summarized. In the shallow crust friction mechanisms (constant Q), fluid flow and scattering all contribute to attenuation. With increasing depth the effects of friction and fluid flow decrease rapidly. Recent results of Flatté and Wu (1988) indicate that the strong scattering regime may extend to 10–15 km depth.

In terms of numbers applicable to average continental crust in non-tectonic areas without a thick section of recent sediments, the following approximate model can be used:

1. At shallow depth ($h \leq 5$ km) low intrinsic (anelastic) Q with frequency dependence $f^{0.5}$. A

typical value would be $Q = 100f^{0.5}$. Scattering is also important in this region.

2. In the lower crust high anelastic Q ($Q_0 \geq 1000$). The influence of scattering may be moderate and remains to be determined in this region.

These values are consistent with models proposed by Campillo et al. (1985) for frequency dependent attenuation in the crust in central France based on Lg waves, and with the results shown in Figure 8. This model is also consistent with the model of lithospheric heterogeneities derived by Flatté and Wu (1988) using travel time and amplitude fluctuations at the Norwegian Seismic Array (NORSAR). In their model the upper crust to a depth of 15 km is rich in small (less than 1 km scale size) heterogeneities, while below that both small and intermediate scale heterogeneities are found to about 200 km depth. The strongly heterogeneous nature of the upper crust has also been confirmed by reflection and refraction profiling (Mooney and Brocher, 1987).

Acknowledgements

This work was supported by the United States Geological Survey under contract number 14-08-0001-G1092 and by the Advanced Research Project Agency of the Department of Defense and monitored by the Air Force Geophysical Laboratory under contract number F19628-86-K-0004. The views expressed in this report, however, are solely those of the authors and do not necessarily represent the views of the United States Geological Survey, the Advanced Research Projects Agency, the Air Force Geophysical Laboratory, or the United States Government.

REFERENCES

Aki, K. (1980), *Attenuation of shear waves in the lithosphere for frequencies from 0.05 to 25 Hz,* Phys. Earth Planet. Inter. *21,* 50–60.

Aki, K., and Chouet, B. (1975), *Origin of coda waves: source, attenuation and scattering effects,* J. Geophys. Res. *80,* 3322–3342.

Aki, K., and Richards, P.G., *Quantitative seismology. Theory and methods* (W.H. Freeman and Co., San Francisco 1980).

Birch, F., and Bancroft, D. (1938), *Elasticity and internal friction in a long column of granite,* Bull. Seism. Soc. Am. *28,* 243–254.

Bradley, J.J., and Fort, A.N., Jr., *Internal friction in rocks,* In *Handbook of Physical constants* (ed. Clark, S.P., Jr.) (1966) pp. 175–193.

Campillo, M., Plantet, J.-L., and Bouchon, M. (1985), *Frequency-dependent attenuation in the crust beneath central France from Lg waves: data analysis and numerical modeling,* Bull. Seism. Soc. Am. *75,* 1395–1411.

Clark, V.A., Spencer, T.W., Tittmann, B.R., Ahlberg, L.A., and Coombe, L.T. (1980), *Effect of volatiles on attenuation Q^{-1} and velocity in sedimentary rocks,* J. Geophys. Res. *85,* 5190–5198.

Dainty, A.M. (1981), *A scattering model to explain seismic Q observations in the lithosphere between 1 and 30 Hz,* Geophys. Res. Lett. *8,* 1126–1128.

Dainty, A.M. (1984), *High-frequency acoustic backscattering and seismic attenuation,* J. Geophys. Res. *89,* 3172–3176.

Dainty, A.M., and Toksöz, M.N. (1977), *Elastic wave propagation in a highly scattering medium. A*

diffusion approach, J. Geophys. *43,* 375–388.

Dainty, A.M., and Toksöz, M.N. (1981), *Seismic codas on the Earth and the Moon: a comparison,* Phys. Earth and Plan. Int. *26,* 250–260.

Dainty, A.M., Toksöz, M.N., and Stein, S. (1976), *Seismic investigation of the lunar interior,* Lunar Science Conf., 7th Proc., Geochim. et Cosmochim. Acta, suppl. 7 *8,* 3057–3075.

Dainty, A.M., Duckworth, R.M., and Tie, A. (1987), *Attenuation and backscattering from local coda,* Bull. Seism. Soc. Am. 77, 1728–1747.

Doll, W.E., Luetgert, J.H., and Murphy, J.M. (1986), *Seismic refraction and wide-angle reflection in the northern Appalachians; the Chain Lakes Massif, northwest Maine (abst.),* EOS *67,* 312.

Flatté, S.M., and Wu, R.S. (1988), *Small-scale structure in the lithosphere and asthenosphere deduced from arrival time and amplitude fluctuations at NORSAR,* J. Geophys. Res., in press.

Frankel, A., and Clayton, R.W. (1986), *Finite difference simulations of seismic scattering: implications for the scattering of short-period seismic waves in the crust and models of crustal heterogeneity,* J. Geophys. Res. *91,* 6465–6489.

Gao, L.S., Lee, L.C., Biswas, N.H., and Aki, K. (1983a), *Comparison of the effects between single and multiple scattering on coda waves for local earthquakes,* Bull. Seism. Soc. Am. *73,* 373–389.

Gao, L.S., Lee, L.C., Biswas, N.H., and Aki, K. (1983b), *Effects of multiple scattering on coda waves in three-dimensional medium,* PAGEOPH *121,* 3-15.

Gardner, G.H.F., Wyllie, M.R.J., and Droschack, D.M. (1964), *Effects of pressure and fluid saturation on the attenuation of elastic waves in sands,* J. Petr. Tech., 189–198.

Gupta, I.N., Burnetti, A., McElfresh, T.W., Von Seggern, D.H., and Wagner, R.A. (1983), *Lateral*

variations in attenuation of ground motion in the eastern United States based on propagation of Lg, NUREG/CR-3555, U.S. Nuclear Regulatory Commission, Washington, D.C.

Herraiz, M., and Espinosa, A. F. (1987), *Coda waves: a review,* PAGEOPH *125,* 499–577.

Herrmann, R.B. (1980), *Q estimates using the coda of local earthquakes,* Bull. Seism. Soc. Am. *70,* 447–468.

Herrmann, R.B., and Mitchell, B.J. (1975), *Statistical analysis and interpretation of surface-wave anelastic attenuation data for the stable interior of North America,* Bull. Seism. Soc. Am. *65,* 1115–1128.

Johnston, D.H., and Toksöz, M.N. (1980), *Ultrasonic P and S wave attenuation in dry and saturated rocks under pressure,* J. Geophys. Res. *85,* 925–936.

Klima, K., Vanek, J., and Pros, Z. (1964), *The attenuation of longitudinal waves in diabase and greywacke under pressure up to 4 kilobars,* Studia Geoph. et Geod. *8,* 247–254.

Knopoff, L. (1964), *Q*, Rev. Geophys. *2,* 625–660.

Kopnichev, Y.F. (1977), *The role of multiple scattering in the formation of a seismogram tail,* Izv. Acad. Sci., USSR, Phys. Solid Earth *13,* 394–398.

Mason, W.P., Beshers, D.N., and Kuo, J.T. (1970), *Internal friction in Westerly granite: relation to dislocation theory,* J. Appl. Phys. *41,* 5206–5209.

Mitchell, B.J. (1980), *Frequency dependence of shear wave internal friction in the continental crust of eastern North America,* J. Geophys. Res. *85,* 5212–5218.

Mooney, W.D., and Brocher, T.M. (1987), *Coincident seismic reflection/refraction studies of the continental lithosphere: a global review,* Rev. Geophys. *25,* 723–742.

Nur, A., and Winkler, K. (1980). *The role of friction and fluid flow in wave attenuation in rocks (abst.)*, Geophysics *45*, 591–592.

O'Doherty, R.F., and Anstey, N.A. (1971), *Reflections on amplitudes*, Geophys. Prospect. *19*, 430–458.

Pandit, B.I., and Savage, J.C. (1973), *An experimental test of Lomnitz's theory of internal friction in rocks*, J. Geophys. Res. *78*, 6097–6099.

Peselnick, L., and Outerbridge, W.F. (1961), *Internal friction in shear and shear modulus of Solenhofen limestone over a frequency range of* 10^7 *cycles per second*, J. Geophys. Res. *66*, 581–588.

Pulli, J. (1984), *Attenuation of coda waves in New England*, Bull. Seism. Soc. Am. *74*, 1149–1166.

Rautian, T.G., and Khalturin, V.I. (1978), *The use of the coda for the determination of the earthquake source spectrum*, Bull. Seism. Soc. Am. *68*, 1809–1827.

Richards, P.G., and Menke, W. (1983), *The apparent attenuation of a scattering medium*, Bull. Seism. Soc. Am. *73*, 1005–1021.

Roecker, S.W., Tucker, B., King, J., and Hatzfield, D. (1982), *Estimates of Q in central Asia as a function of frequency and depth using the coda of locally recorded earthquakes*, Bull. Seism. Soc. Am. *72*, 129–149.

Rovetta, M.R., Blacic, J.D., and Delaney, J.R. (1987), *Microfracture and crack healing in experimentally deformed peridotite*, J. Geophys. Res. *92*, 12902–12910.

Singh, S. (1985), *Lg and coda wave studies of Eastern Canada*, Ph.D. thesis, Saint Louis University, Missouri.

Singh, S., and Hermann, R.B. (1983), *Regionalization of crustal coda Q in the continental United*

States, J. Geophys. Res. *88,* 527–538.

Smith, D.L., and Evans, B. (1984), *Diffusional crack healing in quartz,* J. Geophys. Res. *89,* 4125—4135.

Spencer, J.W., Jr. (1981), *Stress relaxations at low frequencies in fluid saturated rocks: attenuation and modulus dispersion,* J. Geophys. Res. *86,* 1803–1812.

Tittmann, B.R., Housley, R.M., Alers, G.A., and Cirlin, E.H. (1974), *Internal friction in rocks and its relationship to volatiles on the moon,* Lunar Science Conf., 5th Proc., Geochim. et Cosmochim. Acta, suppl. 5 *3,* 2913–2918.

Tittmann, B.R., Na'ler, H., Clark, V.A., Ahlberg, L.A., and Spencer, T.W. (1981), *Frequency dependence of seismic dissipation in saturated rocks,* Geophys. Res. Lett. *8,* 36–38.

Toksöz, M.N., and Johnston, D.H., (eds), (1981), *Seismic wave attenuation,* Geophysics reprint series No. 2, Society of Exploration Geophysicist.

Toksöz, M.N., Johnston, D.H., and Timur, A. (1979), *Attenuation of seismic waves in dry and saturated rocks. I. Laboratory measurements,* Geophysics *44,* 681–690.

Toksöz, M.N., Wu, R.S., and Schmitt, D.P. (1987), *Physical mechanisms contributing to seismic attenuation in the crust,* Proc. NATO ASI 'Strong Ground Motion Seismology', Ankara, Turkey, 225–247.

Toksöz, M.N., Reiter, E., and Mandal, B. (1988), *Seismic attenuation in the crust,* Proc. 10th Ann. DARPA/AFGL Res. Symp., 127–134.

Walsh, J.B. (1966), *Seismic wave attenuation in rock due to fracture,* J. Geophys. Res. *17,* 2591–2599.

Winkler, K., and Nur, A. (1979), *Pore fluids and seismic attenuation in rocks*, Geophys. Res. Lett. *6*, 1–4.

Wu, R.S. (1982), *Attenuation of short period seismic waves due to scattering*, Geophys. Res. Lett. *9*, 9–12.

Wu, R.S. (1984), *Multiple scattering and energy transfer of seismic waves and the application of the theory to Hindu Kush region*, In *Seismic wave scattering and the small scale inhomogeneities in the lithosphere* (Chapter 4, Ph.D. thesis, Mass. Inst. Tech., Cambridge, MA).

Wu, R.S. (1985), *Multiple scattering and energy transfer of seismic waves. Separation of scattering effect from intrinsic attenuation. I. Theoretical modelling*, Geophys. J. R. Astr. Soc. *82*, 57–80.

Wu, R.S., and Aki, K. (1987), *Multiple scattering and energy transfer of seismic waves—separation of scattering effect from intrinsic attenuation. II. Application of the theory to the Hindu Kush region*. This issue.

APPENDIX A

The elastic wave energy received by an isotropic point receiver in a random heterogeneous medium can be represented by the *average energy density* $E(\underline{r})$ at that point. The energy density in radiative transfer theory is defined as (see Wu, 1985):

$$E(\underline{r}) = \frac{1}{C}\int_{4\pi} I(\underline{r},\hat{\Omega})d\Omega \qquad (A-1)$$

where C is the wave velocity, and $I(\underline{r},\hat{\Omega})$ is the *specific intensity or directional intensity.* It gives the power flowing within a unit solid angle in the direction $\hat{\Omega}$ ($\hat{\Omega}$ is the unit vector) received by a unit area perpendicular to $\hat{\Omega}$, in a unit frequency band. The specific intensity is defined for a frequency ω, which is omitted in the notation. Since the P wave energy is much smaller than the S wave energy for earthquakes, we consider here $I(\underline{r},\hat{\Omega})$ as only the S wave energy by neglecting the mode converted energy from P waves. We assume here also that the wave energy described by $I(\underline{r},\hat{\Omega})$ is depolarized, i.e. the energy is equally partitioned between the two orthogonal components of S waves. This agrees generally with the observations.

From the radiative transfer equations we can obtain the equation for the transfer energy density:

$$E(\underline{r}) = E_{in}e^{-\eta_s l} + \int_V \left[\eta_s E(\underline{r}_1) + \varepsilon(\underline{r}_1,\hat{\Omega})\right] G_0(\underline{r}-\underline{r}_1)dV_1 \qquad (A-2)$$

where E_{in} is the incident field and,

$$\varepsilon(\underline{r}_1,\hat{\Omega}) = \frac{4\pi}{C}W(\underline{r}_1,\hat{\Omega}) \qquad (A-3)$$

is the source energy density function, where W is the source power spectral density, and

$$G_0(\underline{r}_1-\underline{r}) = \frac{e^{-\eta_s R}}{4\pi R^2} = \frac{e^{-\eta_s|\underline{r}-\underline{r}_1|}}{4\pi\,|\underline{r}-\underline{r}_1|^2} \qquad (A-4)$$

In (A-2), suppose the incident field $E_{in} = 0$ and the isotropic point source is located at $\underline{r} = 0$, radiating total power P_0. Then,

$$\epsilon(\underline{r}) = \frac{P_0}{C}\delta(\underline{r}) = E_0\delta(\underline{r}) \qquad (A-5)$$

and Equation (A-2) becomes:

$$E(\underline{r}) = E_0\frac{e^{-\eta_e r}}{4\pi r^2} + \int_V \eta_s E(r_1)\frac{e^{-\eta_e|\underline{r}-\underline{r}_1|}}{4\pi\ \underline{r}-\underline{r}_1\ ^2}dV_1 \qquad (A-6)$$

Assuming $E_0 = 1$, the solution can be written as:

$$\begin{aligned} E(\underline{r}) &= \frac{\eta_e P_d}{4\pi r}\exp(-\eta_e d_0 r) + \frac{\eta_e}{4\pi r}\int_1^\infty f(s, B_0)\exp(-\eta_e r s)ds \\ &= E_d(r) + E_c(r) \end{aligned} \qquad (A-7)$$

where

$$P_d = \frac{2d_0^2(1-d_0^2)}{B_0(d_0^2 + B_0 - 1)} \qquad (A-8)$$

and d_0 is the diffuse multiplier determined by:

$$\frac{B_0}{2d_0}\ln\left\{\frac{1+d_0}{1-d_0}\right\} = 1; \qquad (A-9)$$

and

$$f(s, B_0) = \left\{\left[1 - \frac{B_0}{s}\tanh^{-1}(\frac{1}{s})\right]^2 + \left(\frac{\pi}{2}\frac{B_0}{s}\right)^2\right\}^{-1} \qquad (A-10)$$

The first term in Equation (A-7) is the diffuse term E_d and the second term is the coherent term E_c.

Note that the diffuse multiplier d_0 is always less than 1. When distance r is large, especially for large B_0, the diffuse term becomes dominant, and $E(r)$ will be approximately an exponential decay with an apparent attenuation coefficient $d_0\eta_e$, which is less than the extinction coefficient η_e.

The degree of reduction depends on the albedo B_0. Figure 1 shows the energy density distribution with distances for different albedo values.

Figure Captions

Figure 1. Normalized energy distribution curves corrected for spherical spreading, $4\pi r^2 E(r)$ as a function of normalized distance $D_e = r/L_e$ where L_e is the extinction length defined by Equation 6 in the text.

Figures 2a,b. Ground velocity (PSV) at 5 Hz (3a) and 1 Hz (2a) as a function of distance for events in northeastern United States and Eastern Canada. Values normalized to a common magnitude. Data are from compilation of Risk Engineering, Inc., under EPRI sponsorship. The solid line in each case is a best fit to data.

△ 11-1-82, New Brunswick, $M - b = 5.5$, ECTN data

○ 19-1-82, New Hampshire, $M_b = 4.8$, strong motion data and ECTN

□ 31-3-82, New Brunswick, $M_b = 4.8$, strong motion data and ECTN

◇ 6-5-82, New Brunswick, $M_b = 4.0$, strong motion data

▲ 16-6-82, New Brunswick, $M_b = 4.6$, strong motion data and ECTN

● 7-10-83, Adirondacks, New York, $M_b = 5.6$, ECTN

■ 11-10-83, Ottawa, Canada, $M_b = 4.1$, ECTN

Figure 3a,b. Match between the multiple scattering model and the observed ground motion data as a function of radial (epicentral) distance R, at frequencies 5 Hz (3a) and 1 Hz (3b). PSV curves are the best fit curves of Figures 2a,b. $(PSV \cdot R/10)$ and $(PSV \cdot R/10)^2$ are calculated from PSV curves. Model and data curves are fit in the distance range of R = 10 to 100 km where model approximations are valid. Results of the fitting are given in Table 1.

Figure 4. Sensitivity of theoretical curves (Power versus radial distance) at $f = 5$ Hz, to different model parameters.

Figure 5. Sensitivity of theoretical curves to albedo (B_o) values at $f = 5$ Hz as a function of distance. Fixed parameters are $L_e = 15$ km, $Q_a = 1350$.

Figure 6. Typical seismograms used in the Rg study. Source-receiver distances are indicated. Rg is the large low-frequency phase.

Figure 7. Observed Rg Q versus frequency and fit (top) and shear Q structures used to fit the data; Q_{0k}, i.e., Q at 1 Hz is shown (bottom). Left: frequency independent $Q = Q_{0k}$ for each layer. Center: $f^{0.5}$ dependence, $Q = Q_{0k}f^{0.5}$ for each layer. Right: f^1 dependence, $Q = Q_{0k}f^1$ for each layer.

Figure 8. Q model for the crust derived from short period Rg data of this study and longer period data of Mitchell (1980). Top: fit to data. Bottom: Q model. Top 2.5 km of the model is the same as Figure 7 (center) with frequency dependence of $Q = Q_0 f^n$, where $n = 0.5$ for $f \geq 0.85$ Hz, and $n = 0$ for $f < 0.85$ Hz. Below 2.5 km Q is independent of frequency.

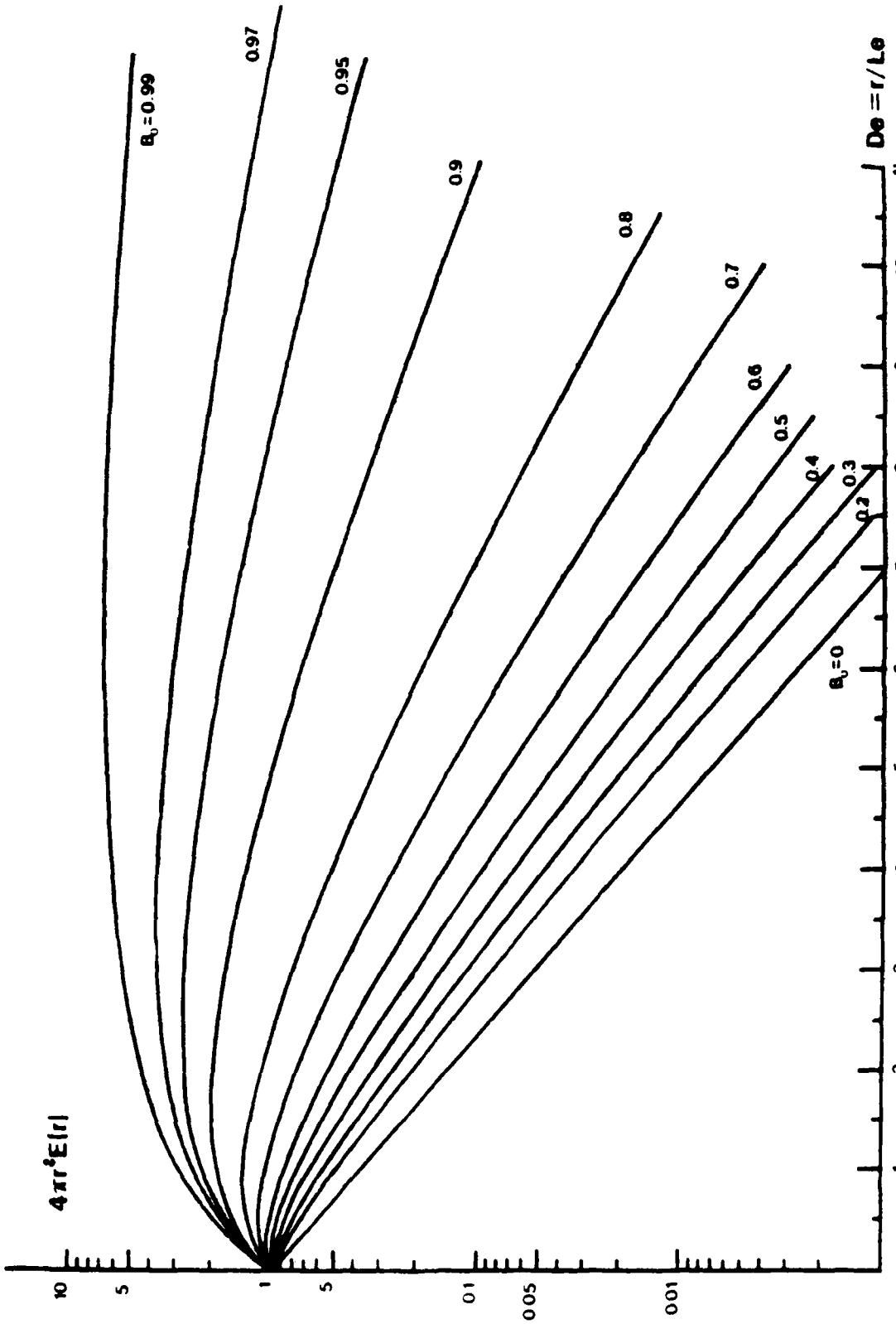
Ω_0=0.99
0.97
0.95
0.9
0.8
0.7
0.6
0.5
0.4
0.3
0.2
Ω_0=0
$4\pi r^4 E(r)$
10
5
1
5
01
005
001
1
2
3
4
5
6
7
8
9
10
11
$D_0 = r/L_0$

Figure 1

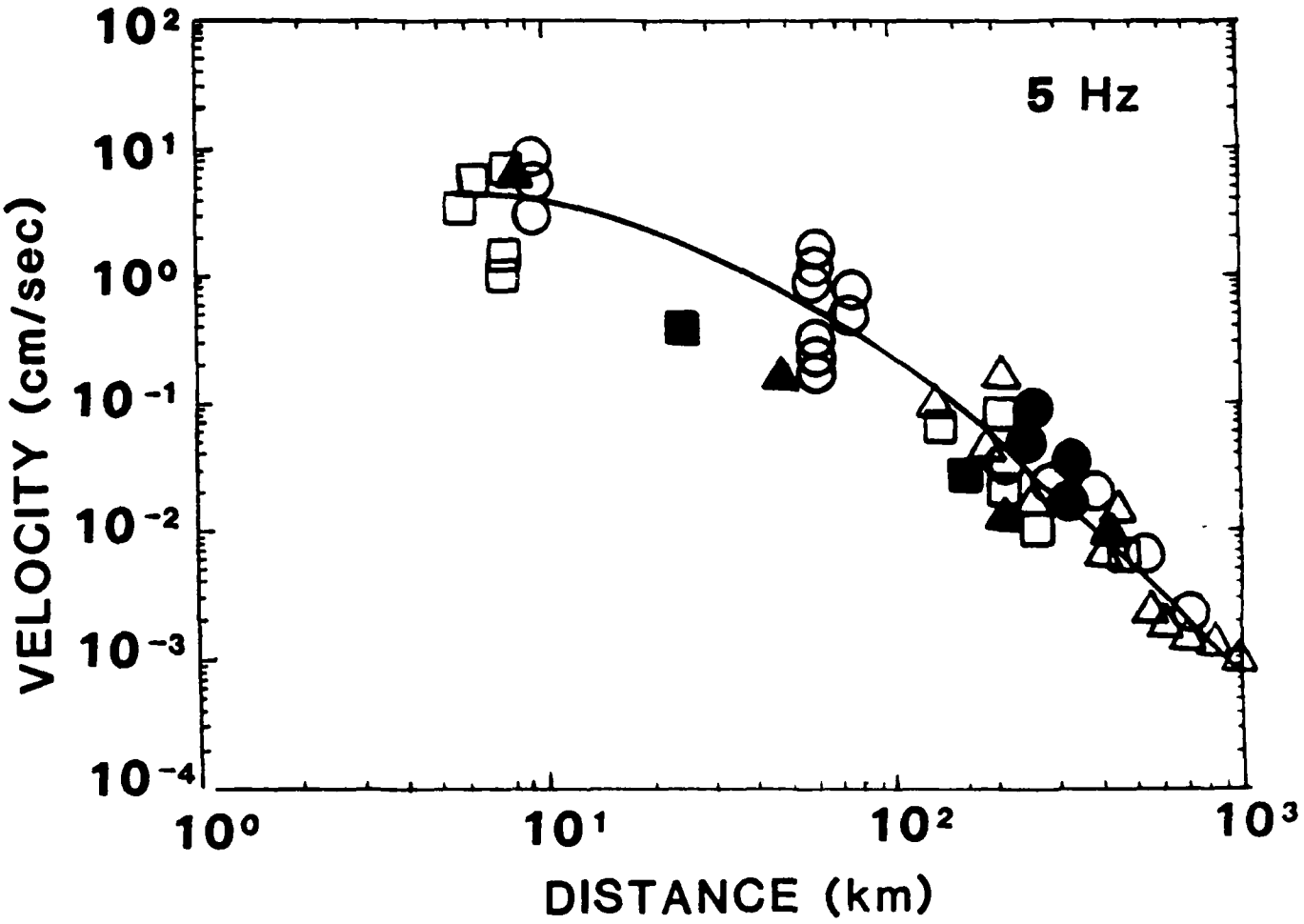
5 Hz
VELOCITY (cm/sec)
10^2
10^1
10^0
10^{-1}
10^{-2}
10^{-3}
10^{-4}
10^0
10^1
10^2
10^3
DISTANCE (km)

Figure 2a

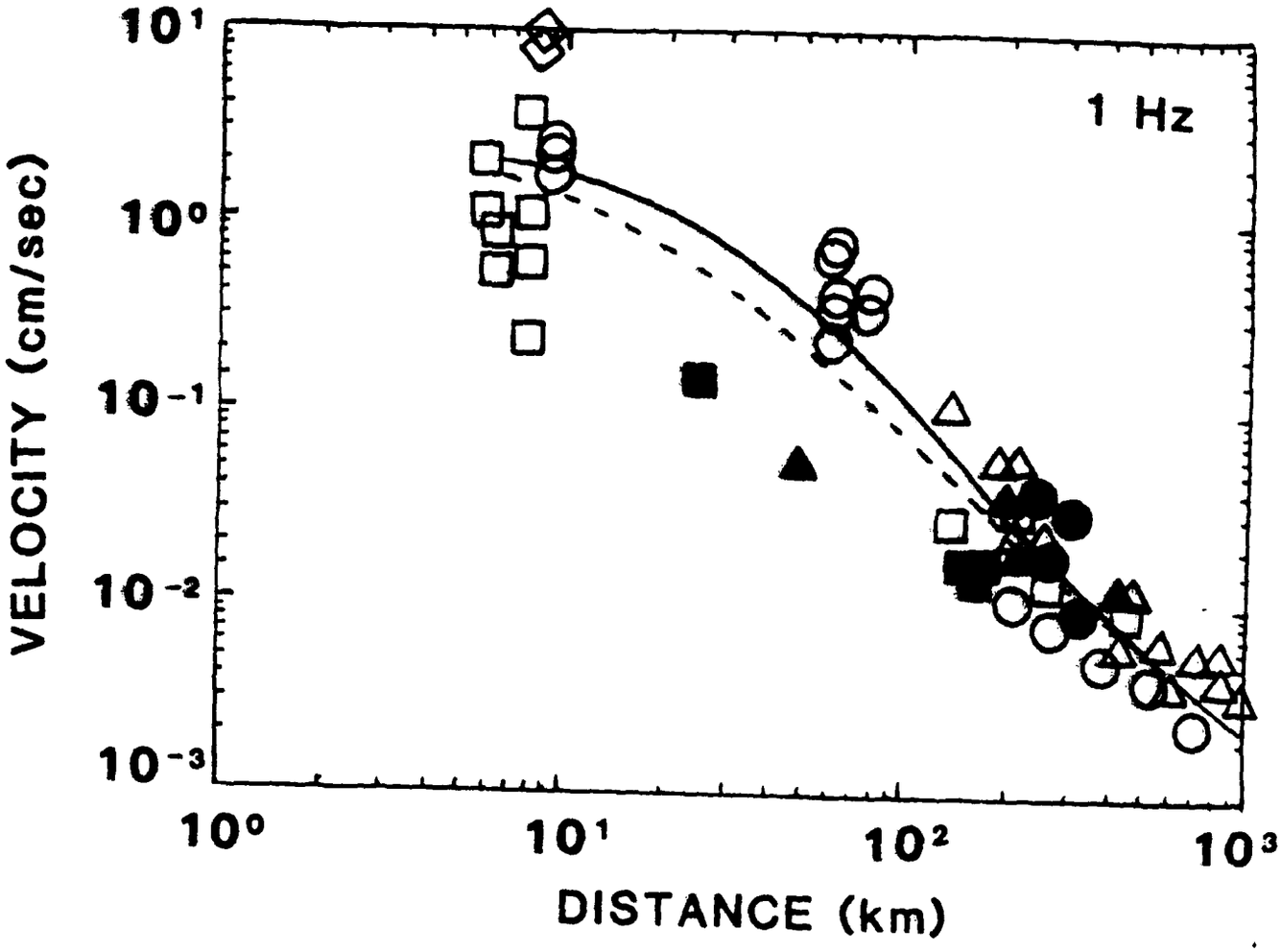
1 Hz
VELOCITY (cm/sec)
DISTANCE (km)
10¹
10⁰
10⁻¹
10⁻²
10⁻³
10⁰
10¹
10²
10³

Figure 2b

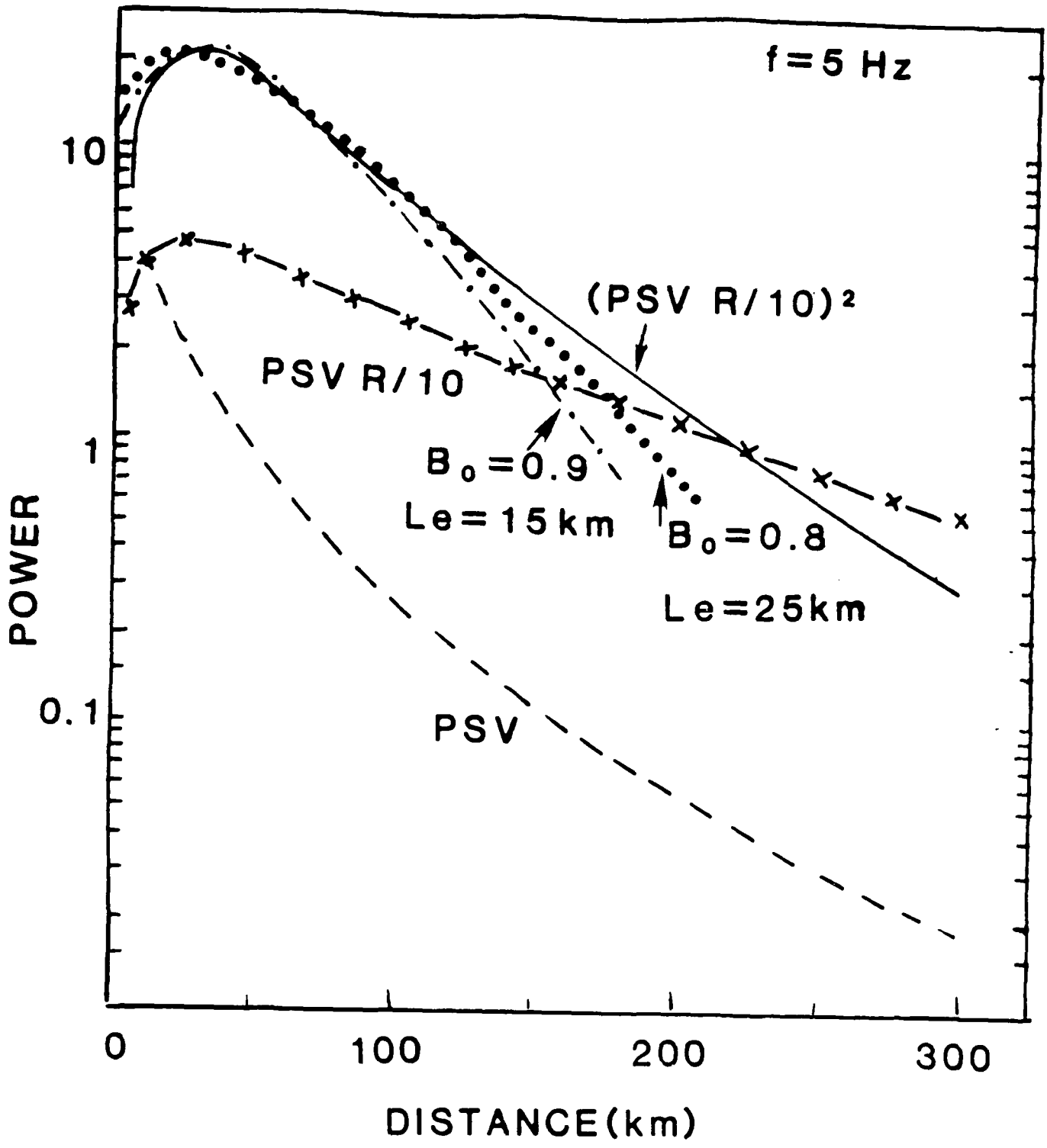
f=5 Hz
10
1
0.1
POWER
(PSV R/10)²
PSV R/10
B₀=0.9
Le=15km
B₀=0.8
Le=25km
PSV
0
100
200
300
DISTANCE(km)

Figur 3a

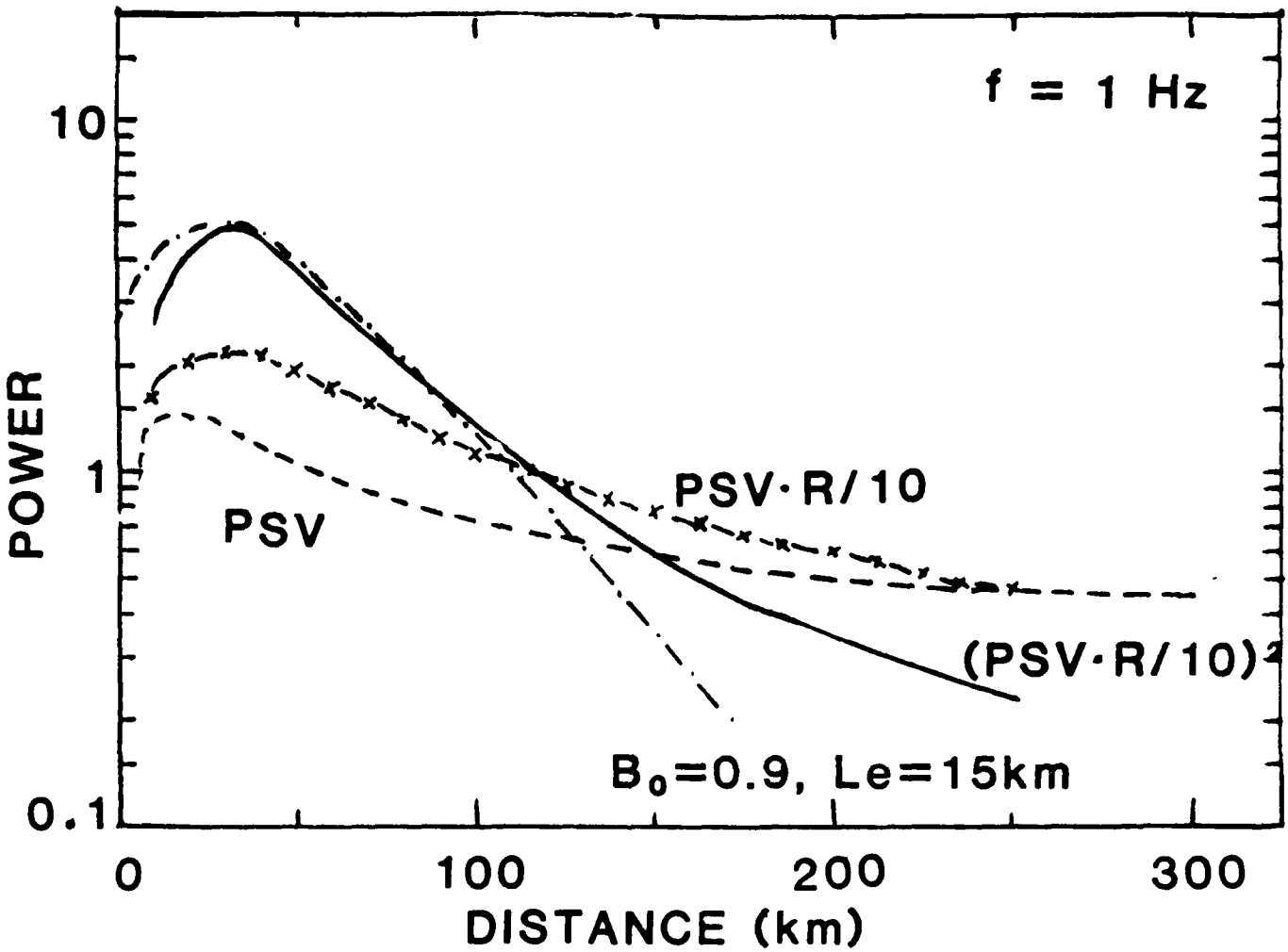
f = 1 Hz
10
1
0.1
POWER
PSV
PSV·R/10
(PSV·R/10)²
B₀=0.9, Le=15km
0
100
200
300
DISTANCE (km)

Figure 3b

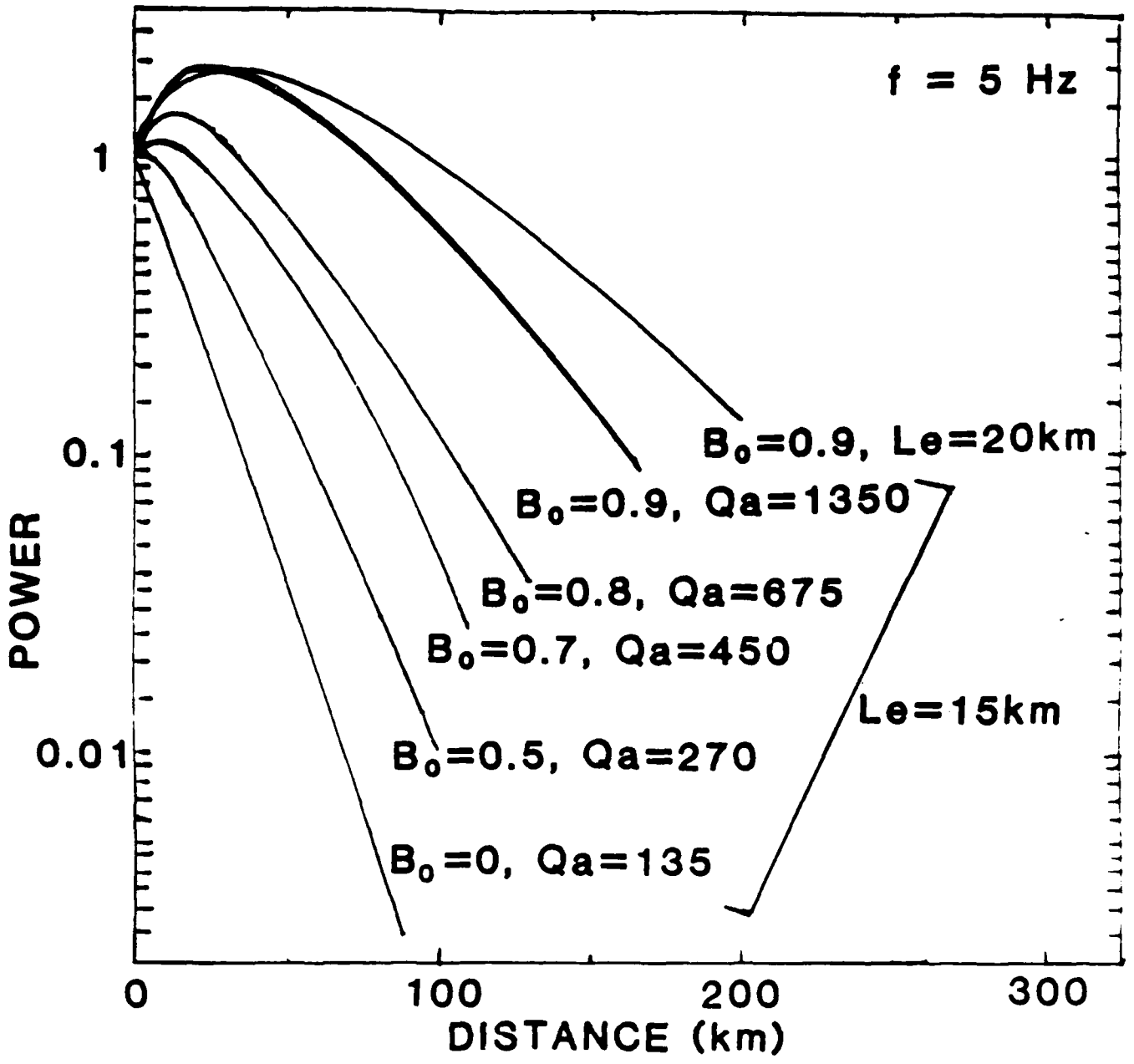
f = 5 Hz
1
0.1
0.01
POWER
B_0=0.9, Le=20km
B_0=0.9, Qa=1350
B_0=0.8, Qa=675
B_0=0.7, Qa=450
Le=15km
B_0=0.5, Qa=270
B_0=0, Qa=135
0
100
200
300
DISTANCE (km)

Figure 4

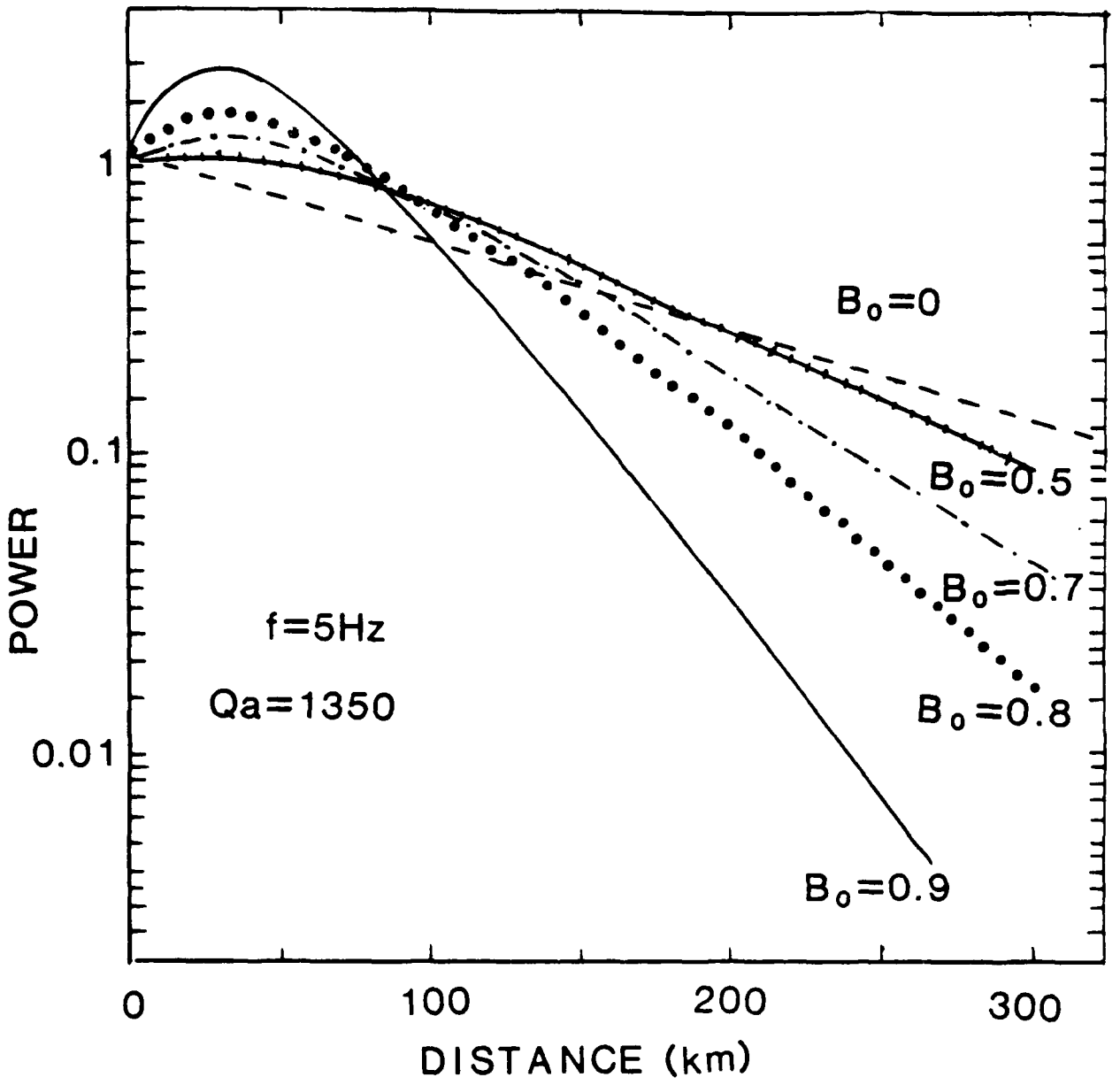
1
0.1
0.01
POWER
f=5Hz
Qa=1350
B_0=0
B_0=0.5
B_0=0.7
B_0=0.8
B_0=0.9
0
100
200
300
DISTANCE (km)

Figure 5

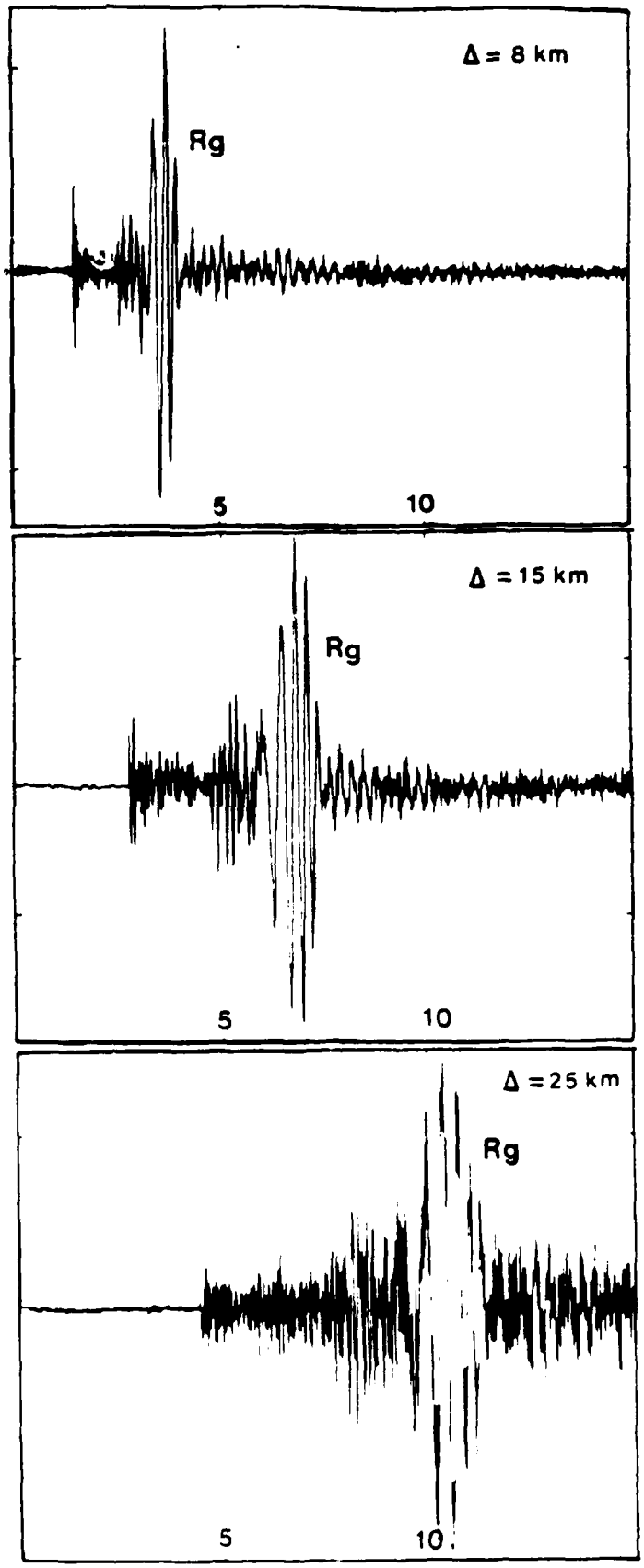

TRAVEL TIME (SEC)

Figure 6

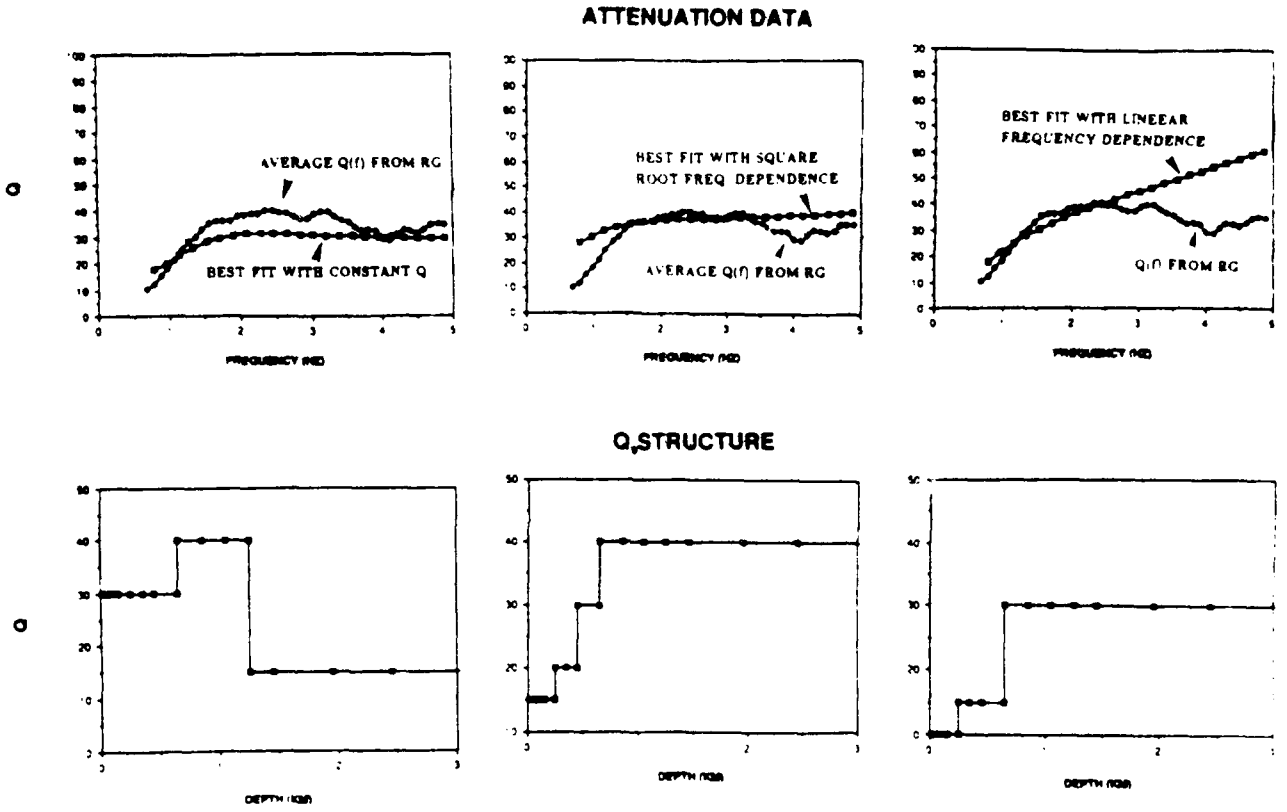
ATTENUATION DATA
Q
AVERAGE Q(f) FROM RG
BEST FIT WITH CONSTANT Q
BEST FIT WITH SQUARE
ROOT FREQ DEPENDENCE
AVERAGE Q(f) FROM RG
BEST FIT WITH LINEEAR
FREQUENCY DEPENDENCE
Q(f) FROM RG
Q,STRUCTURE
Q

Figure 7

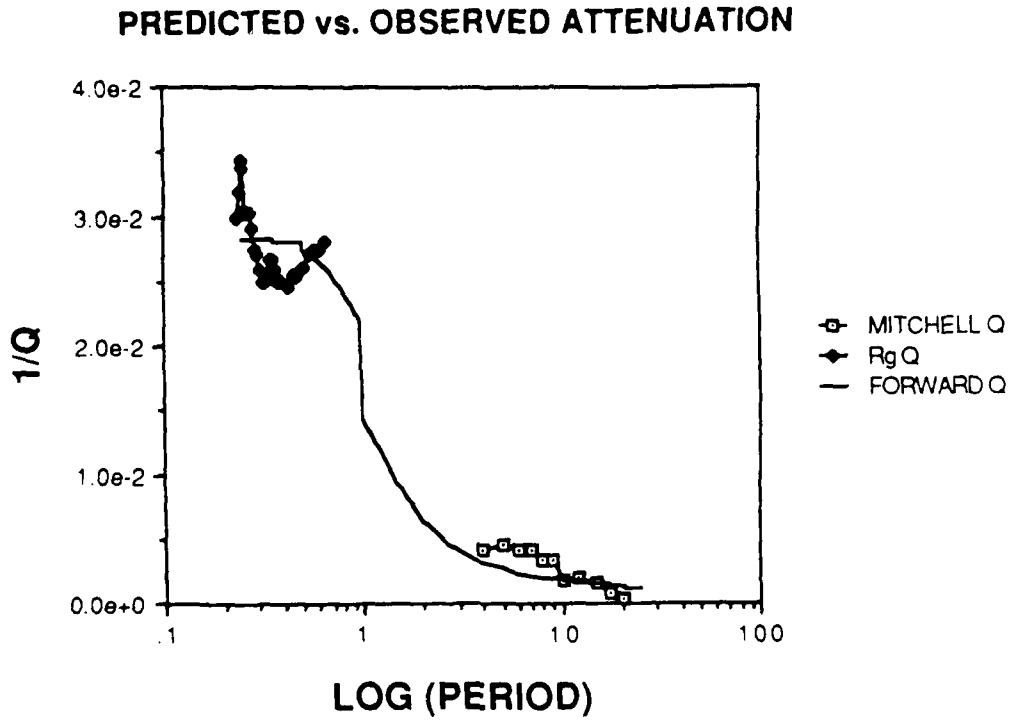
PREDICTED vs. OBSERVED ATTENUATION
4.0e-2
3.0e-2
2.0e-2
1.0e-2
0.0e+0
1/Q
.1
1
10
100
LOG (PERIOD)
MITCHELL Q
Rg Q
FORWARD Q

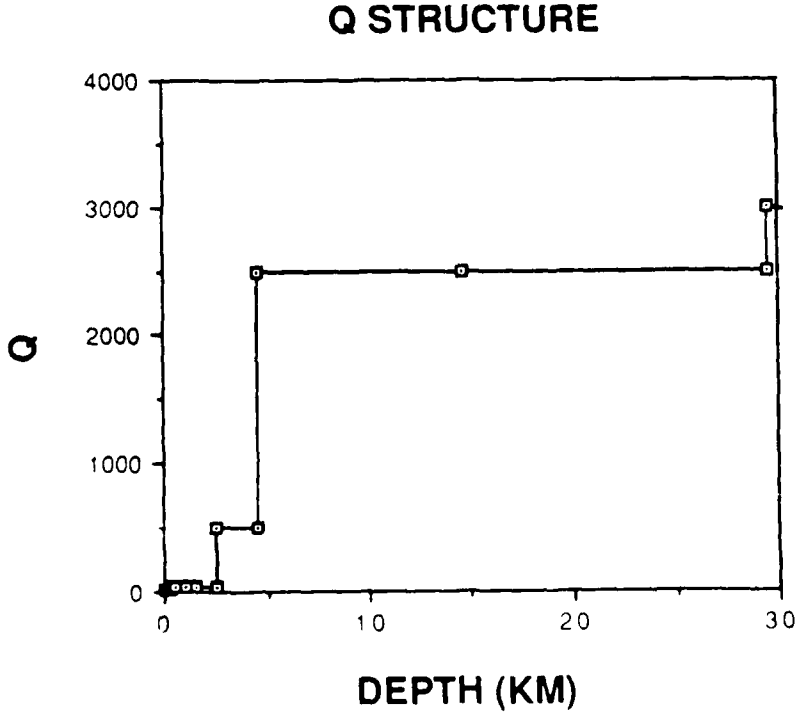
Q STRUCTURE
4000
3000
2000
1000
0
Q
0
10
20
30
DEPTH (KM)

Figure 8

CONTRACTORS (United States)

Professor Keiiti Aki
Center for Earth Sciences
University of Southern California
University Park
Los Angeles, CA 90089-0741

Professor Charles B. Archambeau
Cooperative Institute for Resch
in Environmental Sciences
University of Colorado
Boulder, CO 80309

Dr. Thomas C. Bache Jr.
Science Applications Int'l Corp.
10210 Campus Point Drive
San Diego, CA 92121 (2 copies)

Dr. Douglas R. Baumgardt
Signal Analysis & Systems Div.
ENSCO, Inc.
5400 Port Royal Road
Springfield, VA 22151-2388

Dr. S. Bratt
Science Applications Int'l Corp.
10210 Campus Point Drive
San Diego, CA 92121

Dr. Lawrence J. Burdick
Woodward-Clyde Consultants
P.O. Box 93245
Pasadena, CA 91109-3245 (2 copies)

Professor Robert W. Clayton
Seismological Laboratory/Div. of
Geological & Planetary Sciences
California Institute of Technology
Pasadena, CA 91125

Dr Karl Cogan
N. E. Research
P.O. Box 857
Norwich, VT 05055

Dr. Vernon F. Cormier
Department of Geology & Geophysics
U-45, Roon 207
The University of Conneticut
Storrs, Connecticut 06268

Dr. Zoltan A. Der
ENSCO, Inc.
5400 Port Royal Road
Springfield, VA 22151-2388

Professor John Ferguson
Center for Lithospheric Studies
The University of Texas at Dallas
P.O. Box 830688
Richardson, TX 75083-0688

Professor Stanley Flatte'
Applied Sciences Building
University of California, Santa Cruz
Santa Cruz, CA 95064

Professor Steven Grand
Department of Geology
245 Natural History Building
1301 West Green Street
Urbana, IL 61801

Professor Roy Greenfield
Geosciences Department
403 Deike Building
The Pennsylvania State University
University Park, PA 16802

Professor David G. Harkrider
Seismological Laboratory
Div of Geological & Planetary Sciences
California Institute of Technology
Pasadena, CA 91125

Professor Donald V. Helmberger
Seismological Laboratory
Div of Geological & Planetary Sciences
California Institute of Technology
Pasadena, CA 91125

Professor Eugene Herrin
Institute for the Study of Earth
& Man/Geophysical Laboratory
Southern Methodist University
Dallas, TX 75275

Professor Robert B. Herrmann
Department of Earth & Atmospheric
Sciences
Saint Louis University
Saint Louis, MO 63156

Professor Lane R. Johnson
Seismographic Station
University of California
Berkeley, CA 94720

Professor Thomas H. Jordan
Department of Earth, Atmospheric
and Planetary Sciences
Mass Institute of Technology
Cambridge, MA 02139

Dr Alan Kafka
Department of Geology &
Geophysics
Boston College
Chestnut Hill, MA 02167

Professor Leon Knopoff
University of California
Institute of Geophysics
& Planetary Physics
Los Angeles, CA 90024

Professor Charles A. Langston
Geosciences Department
403 Deike Building
The Pennsylvania State University
University Park, PA 16802

Professor Thorne Lay
Department of Geological Sciences
1006 C.C. Little Building
University of Michigan
Ann Harbor, MI 48109-1063

Dr. Randolph Martin III
New England Research, Inc.
P.O. Box 857
Norwich, VT 05055

Dr. Gary McCartor
Mission Research Corp.
735 State Street
P.O. Drawer 719
Santa Barbara, CA 93102 (2 copies)

Professor Thomas V. McEvilly
Seismographic Station
University of California
Berkeley, CA 94720

Dr. Keith L. McLaughlin
S-CUBED,
A Division of Maxwell Laboratory
P.O. Box 1620
La Jolla, CA 92038-1620

Professor William Menke
Lamont-Doherty Geological Observatory
of Columbia University
Palisades, NY 10964

Professor Brian J. Mitchell
Department of Earth & Atmospheric
Sciences
Saint Louis University
Saint Louis, MO 63156

Mr. Jack Murphy
S-CUBED
A Division of Maxwell Laboratory
11800 Sunrise Valley Drive
Suite 1212
Reston, VA 22091 (2 copies)

Professor J. A. Orcutt
Institute of Geophysics and Planetary
Physics, A-205
Scripps Institute of Oceanography
Univ. of California, San Diego
La Jolla, CA 92093

Professor Keith Priestley
University of Nevada
Mackay School of Mines
Reno, NV 89557

Wilmer Rivers
Teledyne Geotech
314 Montgomery Street
Alexandria, VA 22314

Professor Charles G. Sammis
Center for Earth Sciences
University of Southern California
University Park
Los Angeles, CA 90089-0741

Dr. Jeffrey L. Stevens
S-CUBED,
A Division of Maxwell Laboratory
P.O. Box 1620
La Jolla, CA 92038-1620

Professor Brian Stump
Institute for the Study of Earth & Man
Geophysical Laboratory
Southern Methodist University
Dallas, TX 75275

Professor Ta-liang Teng
Center for Earth Sciences
University of Southern California
University Park
Los Angeles, CA 90089-0741

Professor M. Nafi Toksoz
Earth Resources Lab
Dept of Earth, Atmospheric and
Planetary Sciences
Massachusetts Institute of Technology
42 Carleton Street
Cambridge, MA 02142

Professor Terry C. Wallace
Department of Geosciences
Building #11
University of Arizona
Tucson, AZ 85721

Weidlinger Associates
ATTN: Dr. Gregory Wojcik
620 Hansen Way, Suite 100
Palo Alto, CA 94304
Professor Francis T. Wu
Department of Geological Sciences
State University of new York
At Binghamton
Vestal, NY 13901

OTHERS (United States)

Dr. Monem Abdel-Gawad
Rockwell Internat'l Science Center
1049 Camino Dos Rios
Thousand Oaks, CA 91360

Professor Shelton S. Alexander
Geosciences Department
403 Deike Building
The Pennsylvania State University
University Park, PA 16802

Dr. Ralph Archuleta
Department of Geological Sciences
Univ. of California at Santa Barbara
Santa Barbara, CA

Dr. Muawia Barazangi
Geological Sciences
Cornell University
Ithaca, NY 14853

J. Barker
Department of Geological Sciences
State University of New York at Binghamton
Vestal, NY 13901

Mr. William J. Best
907 Westwood Drive
Vienna, VA 22180

Dr. N. Biswas
Geophysical Institute
University of Alaska
Fairbanks, AK 99701

Dr. G. A. Bollinger
Department of Geological Sciences
Virginia Polytechnical Institute
21044 Derring Hall
Blacksburg, VA 24061

Dr. James Bulau
Rockwell Int'l Science Center
1049 Camino Dos Rios
P.O. Box 1085
Thousand Oaks, CA 91360

Mr. Roy Burger
1221 Serry Rd.
Schenectady, NY 12309

Dr. Robert Burridge
Schlumberger-Doll Resch Ctr.
Old Quarry Road
Ridgefield, CT 06877

Science Horizons, Inc.
ATTN: Dr. Theodore Cherry
710 Encinitas Blvd., Suite 101
Encinitas, CA 92024 (2 copies)

Professor Jon F. Claerbout
Professor Amos Nur
Dept. of Geophysics
Stanford University
Stanford, CA 94305 (2 copies)

Dr. Anton W. Dainty
AFGL/LWH
Hanscom AFB, MA 01731

Dr. Steven Day
Dept. of Geological Sciences
San Diego State U.
San Diego, CA 92182

Professor Adam Dziewonski
Hoffman Laboratory
Harvard University
20 Oxford St.
Cambridge, MA 02138

Professor John Ebel
Dept of Geology & Geophysics
Boston College
Chestnut Hill, MA 02167

Dr. Alexander Florence
SRI International
333 Ravenswood Avenue
Menlo Park, CA 94025-3493

Dr. Donald Forsyth
Dept. of Geological Sciences
Brown University
Providence, RI 02912

Dr. Anthony Gangi
Texas A&M University
Department of Geophysics
College Station, TX 77843

Dr. Freeman Gilbert
Institute of Geophysics & Planetary Physics
Univ. of California, San Diego
P.O. Box 109
La Jolla, CA 92037

Mr. Edward Giller
Pacific Seirra Research Corp.
1401 Wilson Boulevard
Arlington, VA 22209

Dr. Jeffrey W. Given
Sierra Geophysics
11255 Kirkland Way
Kirkland, WA 98033

Dr. Henry L. Gray
Associate Dean of Dedman College
Department of Statistical Sciences
Southern Methodist University
Dallas, TX 75275

Rong Song Jih
Teledyne Geotech
314 Montgomery Street
Alexandria, Virginia 22314

Professor F.K. Lamb
University of Illinois at
Urbana-Champaign
Department of Physics
1110 West Green Street
Urbana, IL 61801

Dr. Arthur Lerner-Lam
Lamont-Doherty Geological Observatory
of Columbia University
Palisades, NY 10964

Dr. L. Timothy Long
School of Geophysical Sciences
Georgia Institute of Technology
Atlanta, GA 30332

Dr. Peter Malin
University of California at Santa Barbara
Institute for Central Studies
Santa Barbara, CA 93106

Dr. George R. Mellman
Sierra Geophysics
11255 Kirkland Way
Kirkland, WA 98033

Dr. Bernard Minster
Institute of Geophysics and Planetary
Physics, A-205
Scripps Institute of Oceanography
Univ. of California, San Diego
La Jolla, CA 92093

Professor John Nabelek
College of Oceanography
Oregon State University
Corvallis, OR 97331

Dr. Geza Nagy
U. California, San Diego
Dept of Ames, M.S. B-010
La Jolla, CA 92093

Dr. Jack Oliver
Department of Geology
Cornell University
Ithaca, NY 14850

Dr. Robert Phinney/Dr. F.A. Dahlen
Dept of Geological
Geophysical Sci. University
Princeton University
Princeton, NJ 08540 (2 copies)

RADIX Systems, Inc.
Attn: Dr. Jay Pulli
2 Taft Court, Suite 203
Rockville, Maryland 20850

Professor Paul G. Richards
Lamont-Doherty Geological
Observatory of Columbia Univ.
Palisades, NY 10964

Dr. Norton Rimer
S-CUBED
A Division of Maxwell Laboratory
P.O. 1620
La Jolla, CA 92038-1620

Professor Larry J. Ruff
Department of Geological Sciences
1006 C.C. Little Building
University of Michigan
Ann Arbor, MI 48109-1063

Dr. Alan S. Ryall, Jr.
Center of Seismic Studies
1300 North 17th Street
Suite 1450
Arlington, VA 22209-2308 (4 copies)

Dr. Richard Sailor
TASC Inc.
55 Walkers Brook Drive
Reading, MA 01867

Thomas J. Sereno, Jr.
Service Application Int'l Corp.
10210 Campus Point Drive
San Diego, CA 92121

Dr. David G. Simpson
Lamont-Doherty Geological Observ.
of Columbia University
Palisades, NY 10964

Dr. Bob Smith
Department of Geophysics
University of Utah
1400 East 2nd South
Salt Lake City, UT 84112

Dr. S. W. Smith
Geophysics Program
University of Washington
Seattle, WA 98195

Dr. Stewart Smith
IRIS Inc.
1616 N. Fort Myer Drive
Suite 1440
Arlington, VA 22209

Rondout Associates
ATTN: Dr. George Sutton,
Dr. Jerry Carter, Dr. Paul Pomeroy
P.O. Box 224
Stone Ridge, NY 12484 (4 copies)

Dr. L. Sykes
Lamont Doherty Geological Observ.
Columbia University
Palisades, NY 10964

Dr. Pradeep Talwani
Department of Geological Sciences
University of South Carolina
Columbia, SC 29208

Dr. R. B. Tittmann
Rockwell International Science Center
1049 Camino Dos Rios
P.O. Box 1085
Thousand Oaks, CA 91360

Professor John H. Woodhouse
Hoffman Laboratory
Harvard University
20 Oxford St.
Cambridge, MA 02138

Dr. Gregory B. Young
ENSCO, Inc.
5400 Port Royal Road
Springfield, VA 22151-2388

OTHERS (FOREIGN)

Dr. Peter Basham
Earth Physics Branch
Geological Survey of Canada
1 Observatory Crescent
Ottawa, Ontario
CANADA K1A 0Y3

Dr. Eduard Berg
Institute of Geophysics
University of Hawaii
Honolulu, HI 96822

Dr. Michel Bouchon - Universite
Scientifique et Medicale de Grenob
Lab de Geophysique - Interne et
Tectonophysique - I.R.I.G.M-B.P.
38402 St. Martin D'Heres
Cedex FRANCE

Dr. Hilmar Bungum/NTNF/NORSAR
P.O. Box 51
Norwegian Council of Science,
Industry and Research, NORSAR
N-2007 Kjeller, NORWAY

Dr. Michel Campillo
I.R.I.G.M.-B.P. 68
38402 St. Martin D'Heres
Cedex, FRANCE

Dr. Kin-Yip Chun
Geophysics Division
Physics Department
University of Toronto
Ontario, CANADA M5S 1A7

Dr. Alan Douglas
Ministry of Defense
Blacknest, Brimpton,
Reading RG7-4RS
UNITED KINGDOM

Dr. Manfred Henger
Fed. Inst. For Geosciences & Nat'l Res.
Postfach 510153
D-3000 Hannover 51
FEDERAL REPUBLIC OF GERMANY

Dr. E. Husebye
NTNF/NORSAR
P.O. Box 51
N-2007 Kjeller, NORWAY

Ms. Eva Johannisson
Senior Research Officer
National Defense Research Inst.
P.O. Box 27322
S-102 54 Stockholm
SWEDEN

Tormod Kvaerna
NTNF/NORSAR
P.O. Box 51
N-2007 Kjeller, NORWAY

Mr. Peter Marshall, Procurement
Executive, Ministry of Defense
Blacknest, Brimpton,
Reading FG7-4RS
UNITED KINGDOM (3 copies)

Dr. Ben Menaheim
Weizman Institute of Science
Rehovot, ISRAEL 951729

Dr. Svein Mykkeltveit
NTNF/NORSAR
P.O. Box 51
N-2007 Kjeller, NORWAY (3 copies)

Dr. Robert North
Geophysics Division
Geological Survey of Canada
1 Observatory crescent
Ottawa, Ontario
CANADA, K1A 0Y3

Dr. Frode Ringdal
NTNF/NORSAR
P.O. Box 51
N-2007 Kjeller, NORWAY

Dr. Jorg Schlittenhardt
Federal Inst. for Geosciences & Nat'l Res.
Postfach 510153
D-3000 Hannover 51
FEDERAL REPUBLIC OF GERMANY

University of Hawaii
Institute of Geophysics
ATTN: Dr. Daniel Walker
Honolulu, HI 96822

FOREIGN CONTRACTORS

Dr. Ramon Cabre, S.J.
c/o Mr. Ralph Buck
Economic Consular
American Embassy
APO Miami, Florida 34032

Professor Peter Harjes
Institute for Geophysik
Rhur University/Bochum
P.O. Box 102148, 4630 Bochum 1
FEDERAL REPUBLIC OF GERMANY

Professor Brian L.N. Kennett
Research School of Earth Sciences
Institute of Advanced Studies
G.P.O. Box 4
Canberra 2601
AUSTRALIA

Dr. B. Massinon
Societe Radiomana
27, Rue Claude Bernard
7,005, Paris, FRANCE (2 copies)

Dr. Pierre Mechler
Societe Radiomana
27, Rue Claude Bernard
75005, Paris, FRANCE

GOVERNMENT

Dr. Ralph Alewine III
DARPA/NMRO
1400 Wilson Boulevard
Arlington, VA 22209-2308

Dr. Robert Blandford
DARPA/NMRO
1400 Wilson Boulevard
Arlington, VA 22209-2308

Sandia National Laboratory
ATTN: Dr. H. B. Durham
Albuquerque, NM 87185

Dr. Jack Evernden
USGS-Earthquake Studies
345 Middlefield Road
Menlo Park, CA 94025

U.S. Geological Survey
ATTN: Dr. T. Hanks
Nat'l Earthquake Resch Center
345 Middlefield Road
Menlo Park, CA 94025

Dr. James Hannon
Lawrence Livermore Nat'l Lab.
P.O. Box 808
Livermore, CA 94550

U.S. Arms Control & Disarm. Agency
ATTN: Dick Morrow
Washington, D.C. 20451

Paul Johnson
ESS-4, Mail Stop J979
Los Alamos National Laboratory
Los Alamos, NM 87545

Ms. Ann Kerr
DARPA/NMRO
1400 Wilson Boulevard
Arlington, VA 22209-2308

Dr. Max Koontz
US Dept of Energy/DP 331
Forrestal Building
1000 Independence Ave.
Washington, D.C. 20585

AFOSR/NP
ATTN: Colonel Jerry J. Perrizo
Bldg 410
Bolling AFB, Wash D.C. 20332-6448

HQ AFTAC/TT
Attn: Dr. Frank F. Pilotte
Patrick AFB, Florida 32925-6001

Mr. Jack Rachlin
USGS - Geology, Rm 3 C136
Mail Stop 928 National Center
Reston, VA 22092

Robert Reinke
AFWL/NTESG
Kirtland AFB, NM 87117-6008

HQ AFTAC/TGR
Attn: Dr. George H. Rothe
Patrick AFB, Florida 32925-6001

Donald L. Springer
Lawrence Livermore National Laboratory
P.O. Box 808, L-205
Livermore, CA 94550

Dr. Lawrence Turnbull
OSWR/NED
Central Intelligence Agency
CIA, Room 5G48
Washington, D.C. 20505

Dr. Thomas Weaver
Los Alamos Scientific Laboratory
Los Almos, NM 97544

AFGL/SULL
Research Library
Hanscom AFB, MA 01731-5000 (2 copies)

Secretary of the Air Force (SAFRD)
Washington, DC 20330
Office of the Secretary Defense
DDR & E
Washington, DC 20330

HQ DNA
ATTN: Technical Library
Washington, DC 20305

Director, Technical Information
DARPA
1400 Wilson Blvd.
Arlington, VA 22209

AFGL/XO
Hanscom AFB, MA 01731-5000

Dr. W. H. K. Lee
USGS
Office of Earthquakes, Volcanoes,
& Engineering
Branch of Seismology
345 Middlefield Rd
Menlo Park, CA 94025

Dr. William Leith
USGS
Mail Stop 928
Reston, VA 22092

Dr. Richard Lewis
Dir. Earthquake Engineering and
Geophysics
U.S. Army Corps of Engineers
Box 631
Vicksburg, MS 39180

Dr. Robert Masse'
Box 25046, Mail Stop 967
Denver Federal Center
Denver, Colorado 80225

R. Morrow
ACDA/VI
Room 5741
320 21st Street N.W.
Washington, D.C. 20451

Dr. Keith K. Nakanishi
Lawrence Livermore National Laboratory
P.O. Box 808, L-205
Livermore, CA 94550 (2 copies)

Dr. Carl Newton
Los Alamos National Lab.
P.O. Box 1663
Mail Stop C335, Group E553
Los Alamos, NM 87545

Dr. Kenneth H. Olsen
Los Alamos Scientific Lab.
Post Office Box 1663
Los Alamos, NM 87545

Howard J. Patton
Lawrence Livermore National Laboratory
P.O. Box 808, L-205
Livermore, CA 94550

Mr. Chris Paine
Office of Senator Kennedy
SR 315
United States Senate
Washington, D.C. 20510

AFGL/LW
Hanscom AFB, MA 01731-5000

DARPA/PM
1400 Wilson Boulevard
Arlington, VA 22209

Defense Technical
Information Center
Cameron Station
Alexandria, VA 22314
(5 copies)

Defense Intelligence Agency
Directorate for Scientific &
Technical Intelligence
Washington, D.C. 20301

Defense Nuclear Agency/SPSS
ATTN: Dr. Michael Shore
6801 Telegraph Road
Alexandria, VA 22310

AFTAC/CA (STINFO)
Patrick AFB, FL 32925-6001

Dr. Gregory van der Vink
Congress of the United States
Office of Technology Assessment
Washington, D.C. 20510

Mr. Alfred Lieberman
ACDA/VI-OA'State Department Building
Room 5726
320 - 21St Street, NW
Washington, D.C. 20451